

---

# A BENCHMARK FOR AI-BASED WEATHER DATA ASSIMILATION

---

A PREPRINT

**Wuxin Wang**

National University of Defense Technology  
wuxinwang@nudt.edu.cn

**Weicheng Ni**

National University of Defense Technology  
niweicheng17@nudt.edu.cn

**Tao Han**

Shanghai Artificial Intelligence Laboratory  
hantao10200@gmail.com

**Taikang Yuan**

National University of Defense Technology  
ytk@nudt.edu.cn

**Xiaoyong Li**

National University of Defense Technology  
sayingxmu@nudt.edu.cn

**Boheng Duan\***

National University of Defense Technology  
bbduan@nudt.edu.cn

**Lei Bai\***

Shanghai Artificial Intelligence Laboratory  
bailei@pjlab.org.cn

**Kaijun Ren\***

National University of Defense Technology  
renkaijun@nudt.edu.cn

October 31, 2024

## ABSTRACT

Recent advancements in Artificial Intelligence (AI) have led to the development of several Large Weather Models (LWMs) that rival State-Of-The-Art (SOTA) Numerical Weather Prediction (NWP) systems. Until now, these models have still relied on traditional NWP-generated analysis fields as input and are far from autonomous. Currently, scientists are increasingly focusing on developing data-driven data assimilation (DA) models for LWMs. To expedite advancements in this field and facilitate the operationalization of data-driven end-to-end weather forecasting systems, we propose DABench, a benchmark constructed by simulated observations, real-world observations, and ERA5 reanalysis. DABench contributes four standard features: (1) sparse and noisy observations provided for both simulated and real-world experiments; (2) a Skillful pre-trained Transformer-based weather prediction model, Sformer, designed to generate background fields while rigorously assessing the impact of assimilation outcomes on predictions; (3) standardized evaluation metrics for the model comparison; (4) a strong DA baseline, 4DVarFormerV2. Our experimental results demonstrate that the end-to-end weather forecasting system, integrating 4DVarFormerV2 and Sformer, can assimilate real-world observations, thereby facilitating a stable DA cycle lasting one year and achieving a skillful forecasting lead time of up to 7 days. The proposed DABench will significantly advance research in AI-based DA, AI-based weather forecasting, and related domains.

**Keywords** benchmark · data assimilation · real-world observations · end-to-end weather forecasting system

---

\*Corresponding author

## Contents

<b>1</b>	<b>Introduction</b>	<b>4</b>
<b>2</b>	<b>Results</b>	<b>5</b>
2.1	The pipeline of developing and evaluating an end-to-end weather forecasting system . . . . .	5
2.2	Results of the deterministic DA and predictions under the OSSE configuration . . . . .	6
2.2.1	One year DA cycle results . . . . .	6
2.2.2	Medium-range weather forecasting results . . . . .	7
2.3	Results of the deterministic DA and predictions under the OSE configuration . . . . .	8
2.3.1	One year DA cycle results . . . . .	8
2.3.2	Medium-range weather forecasting results . . . . .	11
2.4	Results of the ensemble DA . . . . .	11
<b>3</b>	<b>Discussion</b>	<b>13</b>
<b>4</b>	<b>Materials and Methods</b>	<b>16</b>
4.1	General problem definition . . . . .	16
4.2	Datasets . . . . .	17
4.3	Sformer . . . . .	18
4.4	DA baselines . . . . .	18
4.5	EDA configuration . . . . .	18
4.6	Metrics . . . . .	19
<b>A</b>	<b>Overview of the simulated observations</b>	<b>24</b>
<b>B</b>	<b>Details of the benchmark dataset: data and code</b>	<b>24</b>
B.1	Data Structure . . . . .	24
B.2	Code Structure . . . . .	25
<b>C</b>	<b>Detail of our weather prediction model – Sformer</b>	<b>26</b>
C.1	Model Architecture . . . . .	26
C.2	Training Details . . . . .	28
C.2.1	Data Normalization . . . . .	28
C.2.2	Two-Phase Training . . . . .	28
C.2.3	Optimization . . . . .	28
C.2.4	Software and Hardware being Used . . . . .	28
<b>D</b>	<b>Details of the data assimilation baselines</b>	<b>28</b>
D.1	SwinTransformer . . . . .	28
D.2	4DVarNet . . . . .	29
D.3	STDA . . . . .	29
D.4	4DVarFormer . . . . .	30

---

D.5	4DVarFormerV2 . . . . .	31
D.6	Training Details for Baselines . . . . .	31
D.6.1	Data Normalization . . . . .	31
D.6.2	Training . . . . .	31
D.6.3	Optimization . . . . .	31
D.6.4	Software and Hardware being Used . . . . .	32
<b>E</b>	<b>More DA cycle results</b>	<b>32</b>
E.1	More details of the OSSE results . . . . .	32
E.2	More details of the OSE results . . . . .	34
<b>F</b>	<b>More medium-range forecasting results</b>	<b>35</b>

## 1 Introduction

Understanding and predicting changes in the Earth system has long been a fundamental pursuit of humanity [1]. The rapid advancement of Artificial Intelligence (AI) has led to the emergence of several Large Weather Models (LWMs), such as FourCastNet [2], Pangu [3], GraphCast [4], FuXi [5], and FengWu [6]. These models have demonstrated performance comparable to traditional Numerical Weather Prediction (NWP) systems, such as the Integrated Forecasting System (IFS) developed by the European Centre for Medium-Range Weather Forecasts (ECMWF). However, these AI-based models currently require the analysis fields generated by traditional data assimilation (DA) systems as input, termed “initial fields”. Thus, they are unable to operationalize autonomously as a single system for stable cycling forecasts [7, 8]. Recent research underscores the crucial role of the quality of the initial field in influencing the accuracy of the LWMs [9]. A pivotal question arises: Can AI generate accurate initial fields to initialize LWMs? Addressing this question is essential for accelerating the development of data-driven end-to-end weather prediction systems.

The exploration of data-driven DA methods dates back to 2016 when a study applied a Multilayer Perceptron (MLP) to learn the DA process [10]. Subsequent research further confirmed the viability of AI-based DA using models such as Long Short-Term Memory (LSTM), MLP, Convolutional Neural Network (CNN), and others, individually tested on idealized scenarios like Lorenz 63/96 physical models [11–15] or single-variable applications such as sea surface height (SSH) reconstruction [12, 16]. To operationalize the rapidly evolving LWMs, several studies have implemented AI-based DA models to generate accurate three-dimensional multivariable initial conditions [8, 17, 18]. A notable example is the Adas model [8], introduced by the Shanghai AI Laboratory, designed to assimilate sparse observations and provide initial fields to initialize the FengWu model [6] to produce skillful forecasts. Concurrently, Huang et al. [17] proposed a novel approach using the pre-trained GraphCast [4] as the backbone of a diffusion model [19], which enables the assimilation of sparse simulated observations to correct errors in short-range forecasts. Moreover, Xu et al. [20] highlighted the effectiveness of the AI-based technique in assimilating FengYun satellite data, demonstrating its capability to mitigate biases in short-range forecasts. Additionally, Wang et al. [18] introduced the 4DVarFormer model, which integrates four-dimensional variational (4DVar) [21] prior knowledge within a Transformer [22] architecture. This allows for the assimilation of observed variables to correct unobserved ones by capturing inter-variable relationships.

Despite promising advances, the diversity of observations and prediction models used in these studies presents challenges. This diversity complicates the objective evaluation of the performance of various DA algorithms. For traditional DA algorithmic research, DA is treated as a mathematical problem. Existing DA benchmarks have been established to evaluate DA algorithms, based primarily on simulated datasets derived from simplified numerical models [23–26]. However, there is a gap in the development of the benchmark tailored specifically for data-driven DA systems, particularly that designed for medium-range weather predictions and incorporating real-world observations. A benchmark is essential for facilitating algorithm comparisons against a common standard, thus promoting method development, especially in emerging research areas. Prominent examples include ImageNet [27], WeatherBench [28], and PDEBench [29]. Furthermore, a standardized benchmark streamlines research efforts for individuals with diverse scientific backgrounds, allowing them to concentrate on a unified research objective [28].

To further advance AI-based DA models and develop end-to-end weather forecasting systems, the benchmark should evaluate several key features of the DA models: (1) the ability to assimilate extremely sparse and noisy observations, (2) the ability to generate analysis fields that can initialize LWMs for skillful forecasts, (3) robust performance when assimilating observations with complex distributions, and (4) the suitability of assimilating real observations for operational applications.

Here, we propose a benchmark named *DABench*. Using ERA5 reanalysis as the reference, we collected and pre-processed prepbufr observations from the Global Data Assimilation System (GDAS) [30]. We also generated simulated observations based on the error levels of these real-world observations for the Observing System Simulation Experiment (OSSE) [31, 32]. The OSSE framework allows us to flexibly test the stability and accuracy of DA models under different observation sparsity. In addition, we also constructed an Observation System Experiment (OSE) using these GDAS prepbufr observations for verifying the potential of DA models in real-world operational scenarios.

To enable researchers to compare the performance of DA models effectively, we present a pre-trained **Skillful transformer**-based weather prediction model, termed Sformer. Using ERA5 reanalysis as the initial field, Sformer achieves a skillful forecast lead time of 9 days. Furthermore, we have updated the recently released State-Of-The-Art (SOTA) DA model, 4DVarFormer [18], to develop 4DVarFormerV2. 4DVarFormerV2 demonstrates superior performance in both OSSE and OSE scenarios. When assimilating GDAS prepbufr observations, the end-to-end weather forecasting system, which combines 4DVarFormerV2 and Sformer, enables a long-range stable DA cycle that lasts for one year. Moreover, this system achieves a skillful forecast lead time of 7 days.

This study and its accompanying code focus on the performance assessment of AI-based DA models and provide an open-source, publicly available, and fully reproducible methodology to train and evaluate the SOTA and future-

developed AI-based DA models. The code is available on this Github repository and the dataset is available at the Baidu Drive.

Overall, our contributions can be summarized as follows:

- The key component of our DABench is the dataset, which includes simulated observations, real-world observations, and ERA5 reanalysis data, thereby facilitating the development and evaluation of data-driven end-to-end weather forecasting systems.
- Along with the dataset, a skillful pre-trained prediction model called Sformer is provided. Sformer is used to validate the impact of the initial fields on predictions. By using Sformer, researchers can have a prediction model to fairly compare their DA methods.
- We propose standardized evaluation metrics for model comparison. Our benchmark assesses both the quality of analysis fields during a one-year deterministic or ensemble DA cycle and the performance of medium-range predictions initialized by these analysis fields.
- We evaluate the performance of open-source DA models against this benchmark and propose an enhanced baseline, named 4DVarFormerV2. Furthermore, we present an example demonstrating the development of a skillful end-to-end weather prediction system using 4DVarFormerV2 and Sformer.

## 2 Results

### 2.1 The pipeline of developing and evaluating an end-to-end weather forecasting system

As illustrated in Figure 1, an end-to-end weather prediction system typically consists of two primary components. The first component is a prediction model that, upon receiving an analysis field as input, generates predictions with lead times from 6 hours to 240 hours (10 days). The second component involves assimilating observations to adaptively adjust the simulation of weather states, ensuring stable and continuous cycling forecasts. In our benchmark, we provide a skillful pre-trained weather forecasting model, Sformer, to construct the first component, while the DA baselines are used to build the second component. We introduce SwinTransformer [33], which is commonly used in LWMs, as a minimalist DA baseline. We select open-source models presented in recent published AI-based DA papers as our baselines, including 4DVarNet [12], STDA [34], and 4DVarFormer [18]. Additionally, we have updated 4DVarFormer to develop a more powerful baseline named 4DVarFormerV2. For details of the above baseline models, see Section 4.4.

In the DA cycle evaluation experiments, we assess the performance of the 12-hourly analysis fields over a year to determine the models’ ability to integrate time-varying background fields and observations. The first background field is derived from a 48-hour prediction using ERA5 reanalysis from 00:00 UTC on December 30, 2022, as the initial field. Following this, the DA cycle begins with this background field at 00:00 UTC on January 1, 2023. In this context, the DA cycle involves assimilating observations throughout the 12-hour DA window (DAW) and performing a 12-hour prediction to establish the background field for the next DAW, and so on. We compute the root mean square error (RMSE) and Bias for the analysis fields generated by deterministic DA. For ensemble DA, we further assess the Continuous Ranked Probability Score (CRPS) and the Spread-Skill Ratio (SSR).

In medium-range weather forecasting experiments, we evaluate the RMSE, the anomaly correlation coefficient (ACC), and the Activity of 10-day predictions initialized from the aforementioned analysis fields. Following WeatherBench [28], the initial fields are selected at intervals of 336 hours, starting at 00:00 UTC on January 1, 2023, and 12:00 UTC on January 8, 2023, separately.

In the following subsections, we highlight 8 “headline” variables chosen from the ECMWF Scorecard:

- Z500: Geopotential at 500 hPa.
- T2M: 2 meter temperature.
- T850, T500: Temperature, at 850 and 500 hPa, respectively.
- MSLP: Mean sea level pressure.
- 10U, 10V: 10 meter vector winds.
- Q700: Specific humidity at 700 hPa.

Detailed information on all evaluated metrics is presented in Section 4.6.

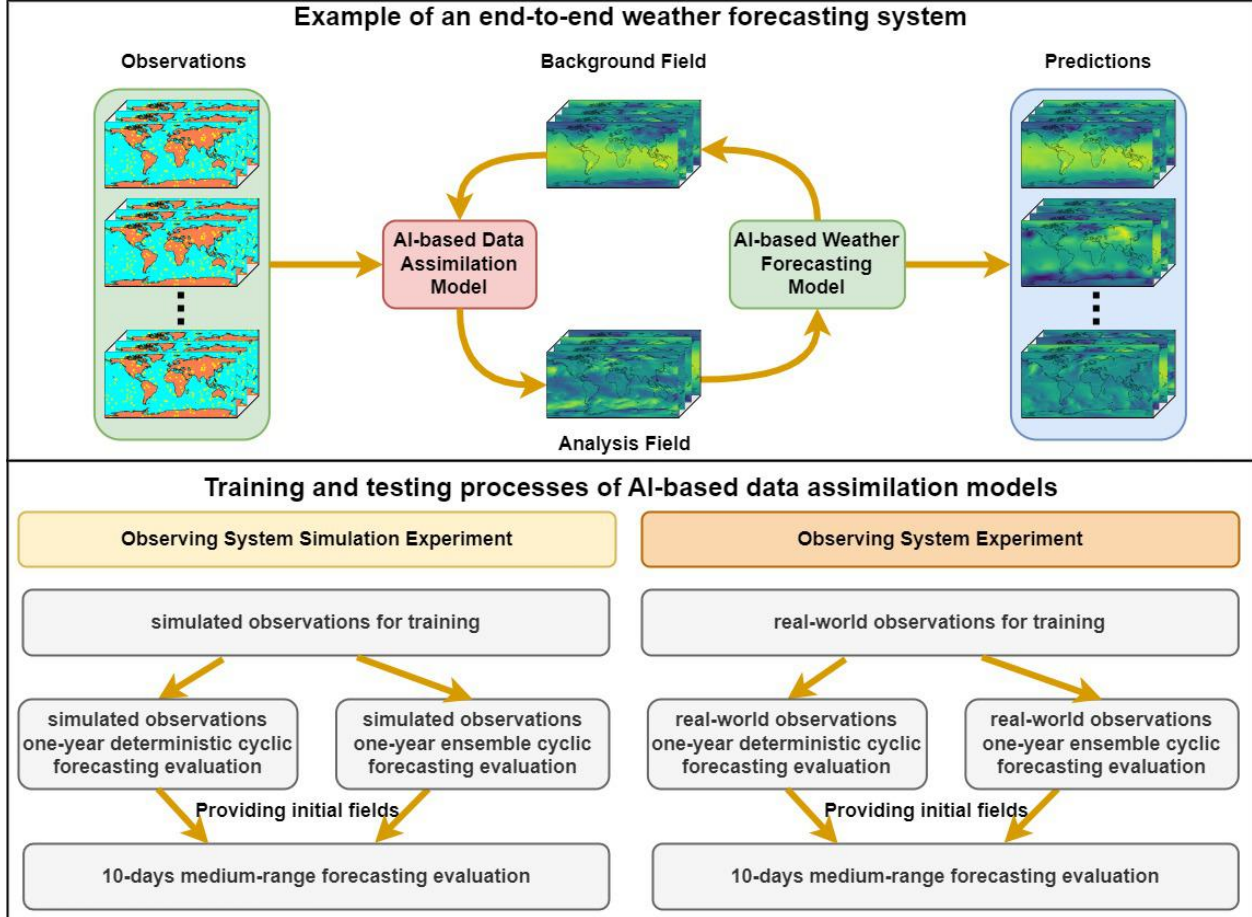


Figure 1: **Schematic diagram of developing and evaluating an end-to-end weather forecasting system.** The system consists of two primary components. First, the prediction component—specifically, the Sformer model presented in this study—performs hierarchical temporal aggregation to generate forecasts. Second, the DA component—comprising the DA baselines assessed in this study—integrates the background field and observations to produce the analysis field necessary for initializing the prediction task. The development and evaluation of the system include both OSSE and OSE configurations. Initially, the assimilation models are trained and evaluated using simulated observations. They are then fine-tuned with real-world observations, ultimately assessing their potential for operationalization in deterministic and ensemble cyclic forecasting settings.

## 2.2 Results of the deterministic DA and predictions under the OSSE configuration

### 2.2.1 One year DA cycle results

We evaluate the performance of baseline models over a one-year DA cycle under the OSSE configuration. The observation mask ratio is set at 90% for both training and testing, which means that only a random 10% of the total grid points are observed. For the first DAW in the DA system, the background field is derived from a 48-hour forecast produced by the Sformer model, initialized with data from the ERA5 reanalysis field. Following this, the alternating weather forecasting and DA steps occur every 12 hours.

Figure 2 shows the annual metrics of the analysis fields generated by DA baselines for our 8 headline variables. Each subplot corresponds to a variable and skill (y-axis) is plotted at 12-hour steps over 365-day horizons (x-axis). Rows 1 and 3 show the RMSE while rows 2 and 4 show the Bias. The original data is represented with reduced opacity to enhance clarity, while solid lines depict values smoothed using an exponential moving average (EMA) with an 11-point window. The results indicate that 4DVarFormerV2 outperforms other baselines for our 8 headline variables throughout the one-year DA cycle. For example, SwinTransformer, 4DVarNet, STDA, and 4DVarFormer generate analysis fields with annual average RMSEs of  $435 \text{ m}^2 \text{ s}^{-2}$ ,  $317 \text{ m}^2 \text{ s}^{-2}$ ,  $685 \text{ m}^2 \text{ s}^{-2}$ , and  $84 \text{ m}^2 \text{ s}^{-2}$  on the Z500, respectively, while 4DVarFormerV2 has only  $64 \text{ m}^2 \text{ s}^{-2}$ . Moreover, the bias for 4DVarFormerV2 remains close to zero throughout the

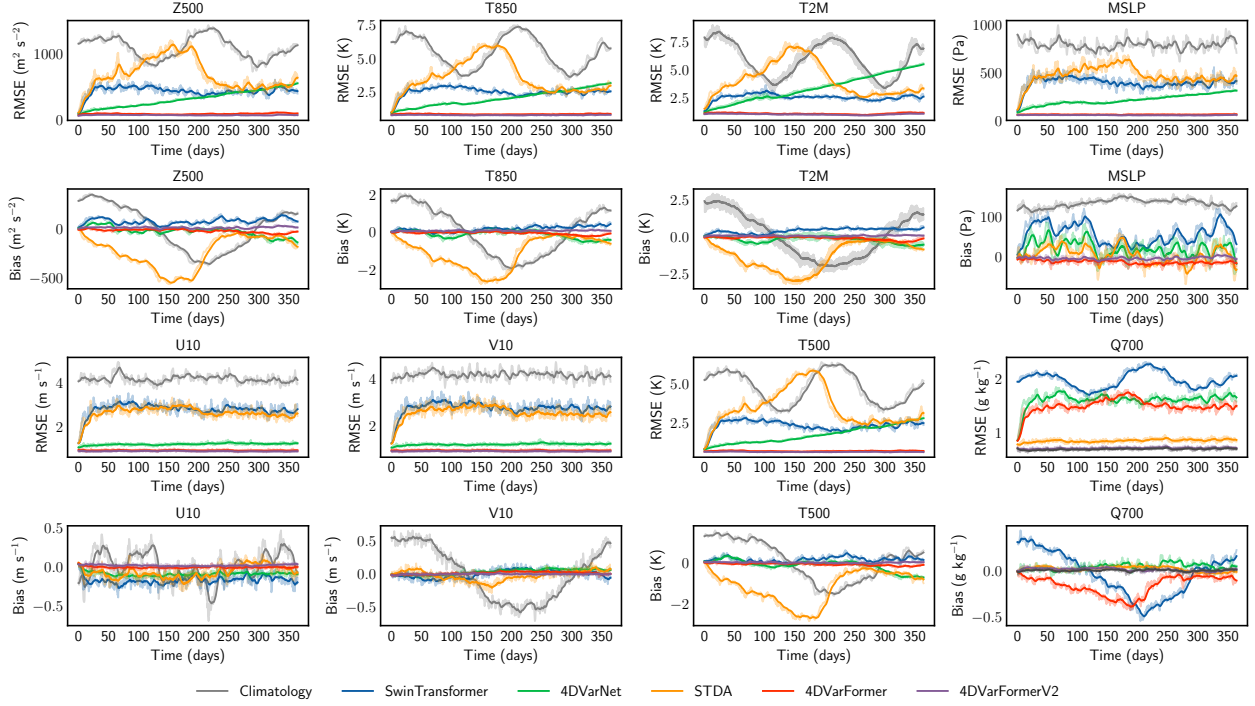


Figure 2: **RMSE and Bias metrics of baselines over a one-year DA cycle under the OSSE configuration.** The RMSEs for the analysis fields are displayed in odd-numbered rows, while the corresponding Bias metrics are displayed in even-numbered rows. The results are color-coded as follows: climatology in gray, the SwinTransformer model in blue, the 4DVarNet model in green, the STDA model in yellow, the 4DVarFormer model in red, and the 4DVarFormerV2 model in purple. These calculations are done for each day of the year at 00:00 UTC and 12:00 UTC. Both RMSE and Bias are computed against ERA5. Each subplot represents a single variable, as indicated in the subplot titles.

year, highlighting its ability to eliminate the bias drift of Sformer. Although climatology exhibits a larger RMSE than 4DVarFormer and 4DVarFormerV2, it does not have significantly large average biases (see Table S2). This may be due to seasonal fluctuations, which is also evident in Figure 2.

Furthermore, this study theoretically evaluates the robustness of the DA baselines trained on 90% masked observations within the complex and varying observation sparsity. We conducted a one-year evaluation of the DA cycle using observations with mask ratios of 90%, 95%, and 99%. The results for 4DVarFormerV2 are presented in Figure 3, where it demonstrates stable RMSEs and Biases over the year across all three mask ratios, indicating its strong robustness in assimilating highly sparse observations to achieve the DA task. The performance of 4DVarFormerV2 diminishes as the mask ratios increase. This result highlights its capability to characterize the contribution of observations to the final analysis field. For the assimilation performance of all baselines at different mask ratios, please see Figures S7 to S10.

## 2.2.2 Medium-range weather forecasting results

Here, we evaluate the impact of the analysis fields derived from the 90% masked OSSE DA cycle on medium-range prediction performance using Sformer. Figure 4 shows how the predictions initialized by 4DVarFormerV2 (purple lines) outperform other baselines for our 8 headline variables. Each subplot corresponds to a variable and skill (y-axis) is plotted at 6-hour steps over 10-day horizons (x-axis). Rows 1 and 4 show RMSE, rows 2 and 5 show ACC, while rows 3 and 6 show Activity. The results show that 4DVarFormerV2 can initialize skillful predictions that extend beyond 8.5 days, which is the maximum lead time at which the ACC of Z500 exceeds 0.6. Notably, the 4DVarFormerV2 model outperforms all DA baselines on our headline variables, suggesting its potential to provide high-quality initial fields for Sformer. For example, the 5-day predictions initialized by climatology, SwinTransformer, 4DVarNet, STDA, and 4DVarFormer achieve RMSEs of  $1131 m^2 s^{-2}$ ,  $859 m^2 s^{-2}$ ,  $593 m^2 s^{-2}$ ,  $1064 m^2 s^{-2}$ , and  $411 m^2 s^{-2}$  on the Z500, respectively, while 4DVarFormerV2 has only  $390 m^2 s^{-2}$ . This result highlights the feasibility of developing a reliable AI-based end-to-end weather prediction system.

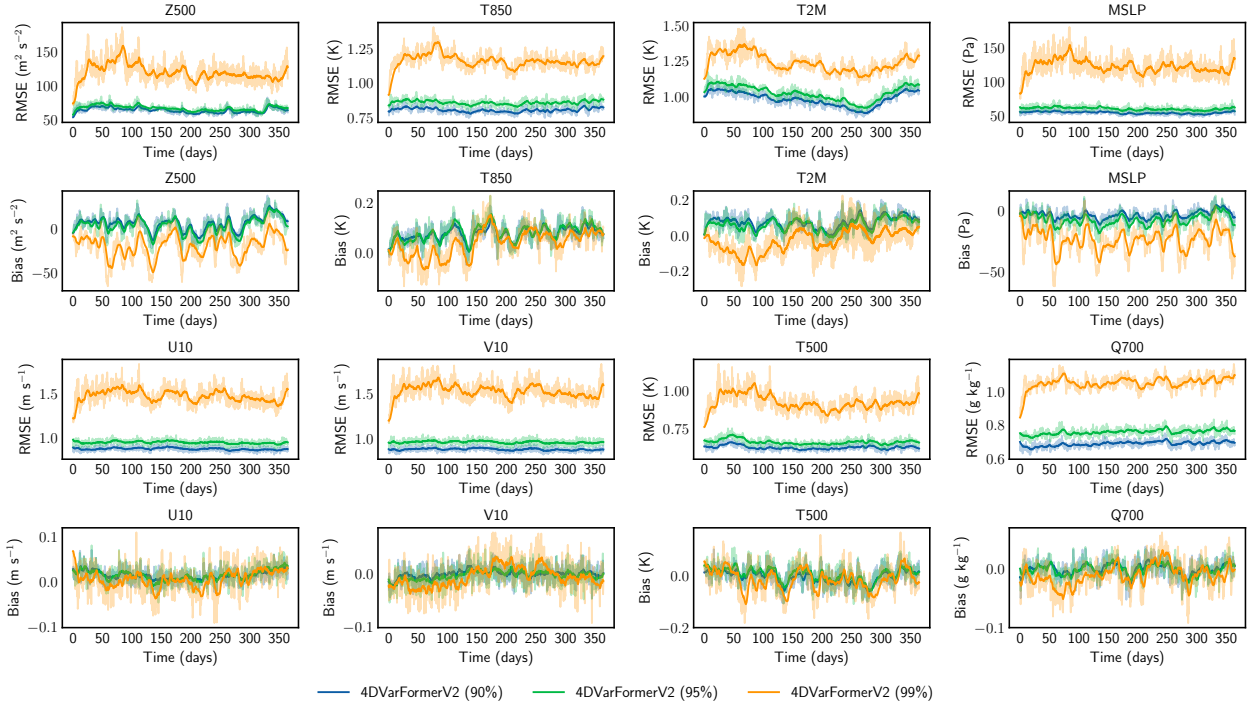


Figure 3: **RMSE and Bias metrics of 4DVarFormerV2 over a one-year DA cycle using different observational mask ratios.** The RMSEs for the analysis fields are displayed in odd-numbered rows, while the corresponding Bias metrics are displayed in even-numbered rows. The results are color-coded as follows: 90% masked results are in blue, 95% masked results are in green, and 99% masked results are in yellow. These calculations are done for each day of the year at 00:00 UTC and 12:00 UTC. Both RMSE and Bias are computed against ERA5. Each subplot represents a single variable, as indicated in the subplot titles.

We further investigate medium-range weather forecasts initiated by the DA baselines while assimilating 90%, 95%, and 99% of masked observations separately. The results for the 4DVarFormerV2 model are illustrated in Figure 5. In particular, the Activities of 4DVarFormerV2 exhibit robust stability across all levels of masked ratios, demonstrating its reliability in estimating extreme values of atmospheric fields, even with limited observations. However, as the proportion of available observations decreases, the corresponding prediction error increases. When 99% of the grid points are masked, the forecast initialized using 4DVarFormerV2 demonstrates a skillful lead time of only 7 days. This emphasizes the necessity for DA models to assimilate as many available observations as possible to develop accurate end-to-end weather forecasting systems.

It is crucial to emphasize that using climatology as the initial field for Sformer in forecasting leads to a gradual increase in Activity. This phenomenon likely arises from climatology’s inherent smoothness, whereas Sformer, trained on ERA5, captures the atmospheric field details. Consequently, when initialized with climatology, Sformer introduces variability that reflects these finer atmospheric details. However, the ACC of forecasts initialized by climatology is close to zero, suggesting that the introduced atmospheric details may not be reliable.

## 2.3 Results of the deterministic DA and predictions under the OSE configuration

### 2.3.1 One year DA cycle results

The spatial and temporal distribution of sounding observations in GDAS prebufr features a higher frequency of observations over land at 00:00 UTC and 12:00 UTC. At other times, upper-air observations over the land are extremely sparse. Consequently, the AI-based DA for real-world observations presents greater challenges than the OSSE configuration. Figure 6 shows the annual metrics of the analysis fields generated by DA baselines for our 8 headline variables. Each subplot corresponds to a variable and skill (y-axis) is plotted at 12-hour steps over 365-day horizons (x-axis). Rows 1 and 3 show RMSE, while rows 2 and 2 show Bias. The original data is represented with reduced opacity to enhance clarity, while solid lines depict values smoothed using an EMA with an 11-point window. The results demonstrate that 4DVarFormerV2 maintains the lowest RMSEs throughout the entire DA cycle over the year,



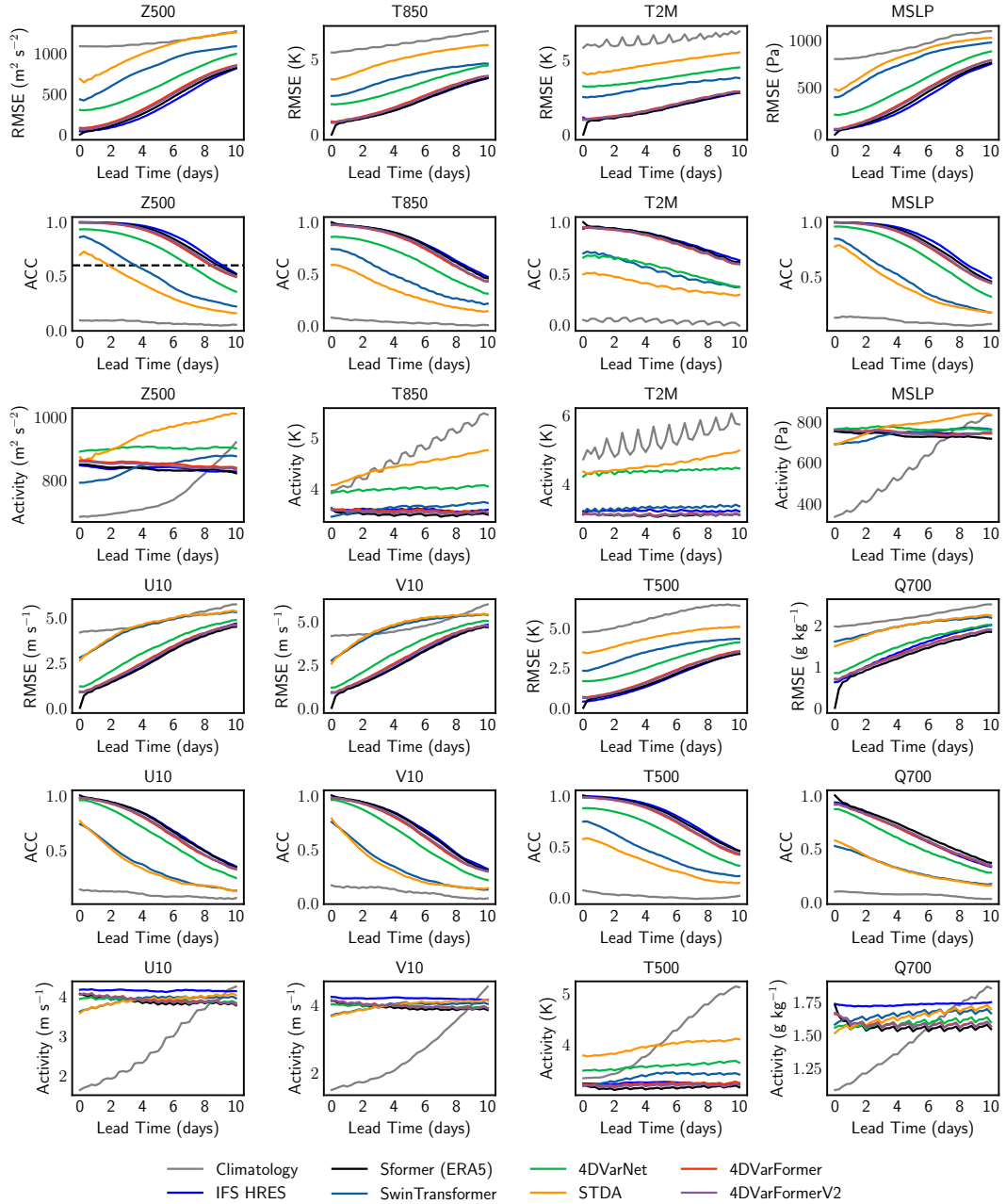


Figure 4: **RMSE, ACC, and Activity metrics of baselines for 10-day medium-range predictions initialized by the analysis fields assimilating 90% masked observations.** The analysis fields produced by the DA models serve as the initial fields for driving the medium-range predictions. The results are color-coded as follows: predictions initialized by climatology in gray, operational predictions of IFS High RESolution (HRES) in dark blue, predictions initialized by ERA5, SwinTransformer, 4DVarNet, STDA, 4DVarFormer, and 4DVarFormerV2 are shown in black, light blue, green, yellow, red, and purple separately. All metrics are computed against ERA5. Each subplot represents a single variable, as indicated in the subplot titles.

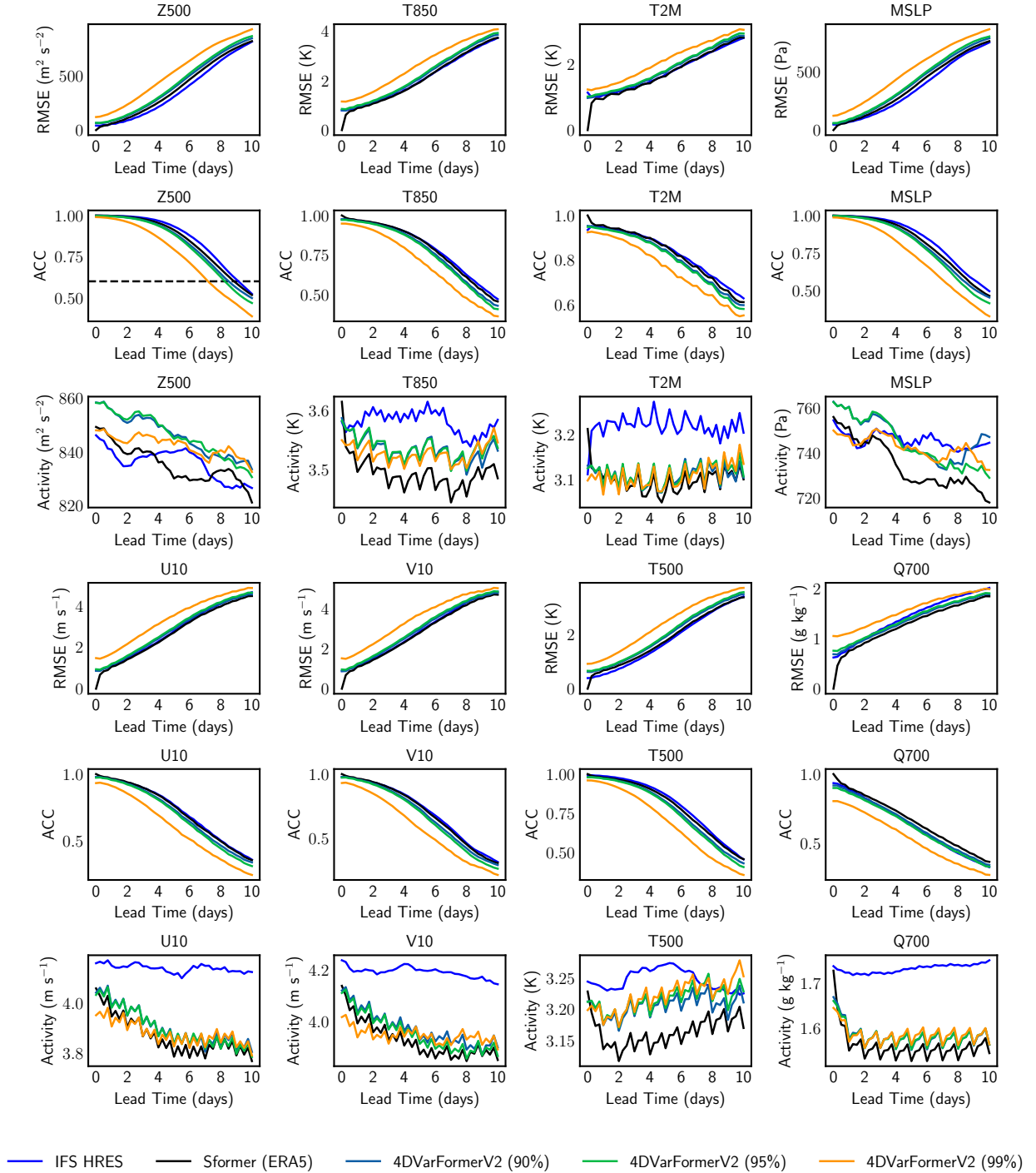


Figure 5: **RMSE, ACC, and Activity metrics of baselines for 10-day medium-range predictions initialized by the analysis fields generated by assimilating 90%, 95%, and 99% masked observations.** The analysis fields produced by the DA models serve as the initial fields for driving the medium-range prediction. The results are color-coded as follows: operational predictions of IFS HRES in dark blue, predictions initialized by ERA5, 4DVarFormerV2 assimilating 90% masked observations, 4DVarFormerV2 assimilating 95% masked observations, and 4DVarFormerV2 assimilating 99% masked observations are shown in black, light blue, green, and yellow separately. All metrics are computed against ERA5. Each subplot represents a single variable, as indicated in the subplot titles.

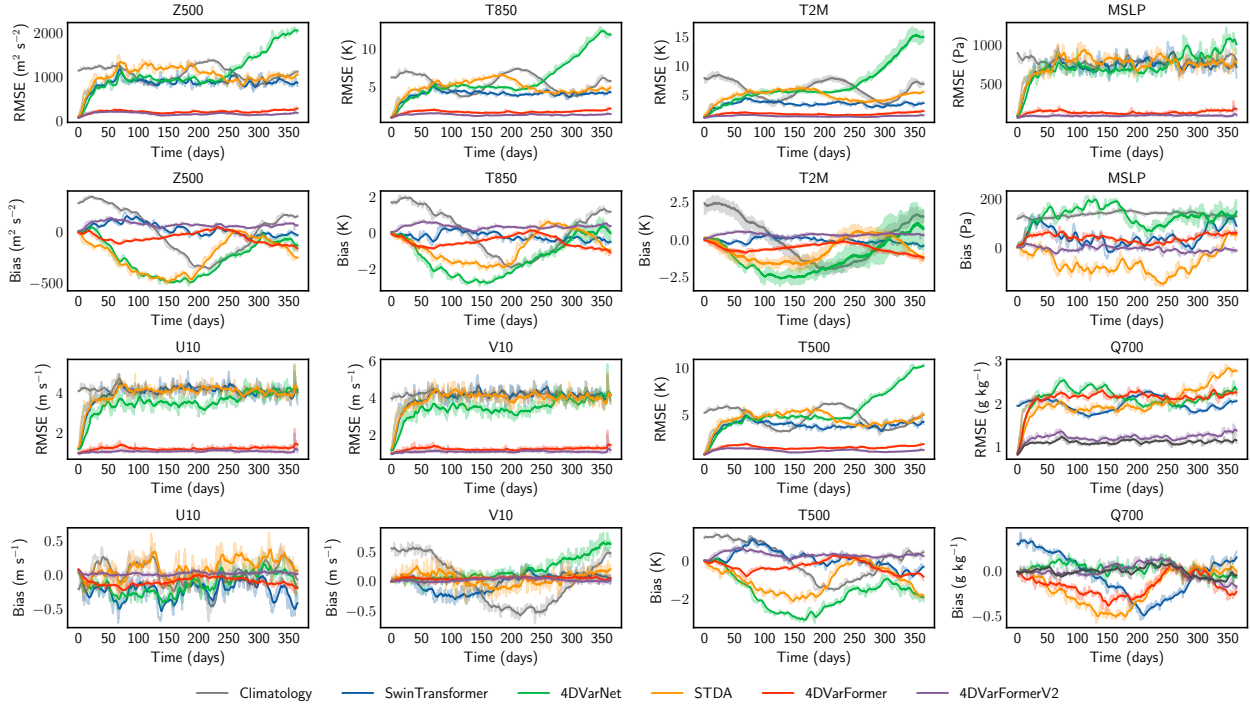


Figure 6: **RMSE and Bias metrics of baselines over a one-year DA cycle under the OSE configuration.** The RMSEs for the analysis fields in 2023 are displayed in odd-numbered rows, while the corresponding Bias metrics are displayed in even-numbered rows. The results are color-coded as follows: climatology in gray, the SwinTransformer model in blue, the 4DVarNet model in green, the STDA model in yellow, the 4DVarFormer model in red, and the 4DVarFormerV2 model in purple. These calculations are done each day of the year at 00:00 UTC and 12:00 UTC. Both RMSE and Bias are computed against ERA5. Each subplot represents a single variable, as indicated in the subplot titles.

indicating its potential for operationalization. For example, SwinTransformer, 4DVarNet, STDA, and 4DVarFormer generate analysis fields with annual average RMSEs of  $873 \text{ m}^2 \text{ s}^{-2}$ ,  $1124 \text{ m}^2 \text{ s}^{-2}$ ,  $1056 \text{ m}^2 \text{ s}^{-2}$ , and  $215 \text{ m}^2 \text{ s}^{-2}$  on the Z500, respectively, while 4DVarFormerV2 achieves only  $167 \text{ m}^2 \text{ s}^{-2}$ . Furthermore, the Bias of 4DVarFormerV2 remains close to zero throughout the year, highlighting its capability to mitigate bias drift from the AI-based forecasting model and prepbufr observations. Similar to the OSSE results, climatology does not exhibit significant average biases due to seasonal fluctuations; however, it shows considerable biases over the time series, as illustrated in Figure 6.

### 2.3.2 Medium-range weather forecasting results

Here, we also evaluated the impact of the analysis fields derived from the OSE DA cycle on medium-range prediction performance using Sformer. Figure 7 illustrates the performance of the medium-range forecast initialized by the analysis fields obtained from assimilating GDAS prepbufr observations. Each subplot corresponds to a variable and skill (y-axis) is plotted at 6-hour steps over 10-day horizons (x-axis). Rows 1 and 4 show RMSE, rows 2 and 5 show ACC, and rows 3 and 6 show Activity. The results indicate that only 4DVarFormer and 4DVarFormerV2 are capable of producing valid medium-range forecasts (with an ACC greater than 0.6 for Z500). Notably, 4DVarFormerV2 can initialize the skillful forecast lead time of Sformer to reach 7 days. This suggests significant potential for the operationalization of 4DVarFormerV2, especially when used in conjunction with the Sformer model, to develop a self-consistent end-to-end weather forecasting system.

## 2.4 Results of the ensemble DA

The ECMWF has operationalized an NWP system that employs ensemble DA (EDA) to generate initial fields [35]. Consequently, evaluating the performance of DA baselines concerning EDA is crucial. To the best of our knowledge, this topic has been addressed in only a limited number of prior studies. In this section, all DA baselines are configured with one control member and ten perturbation members, resulting in a total of eleven ensemble members. For additional

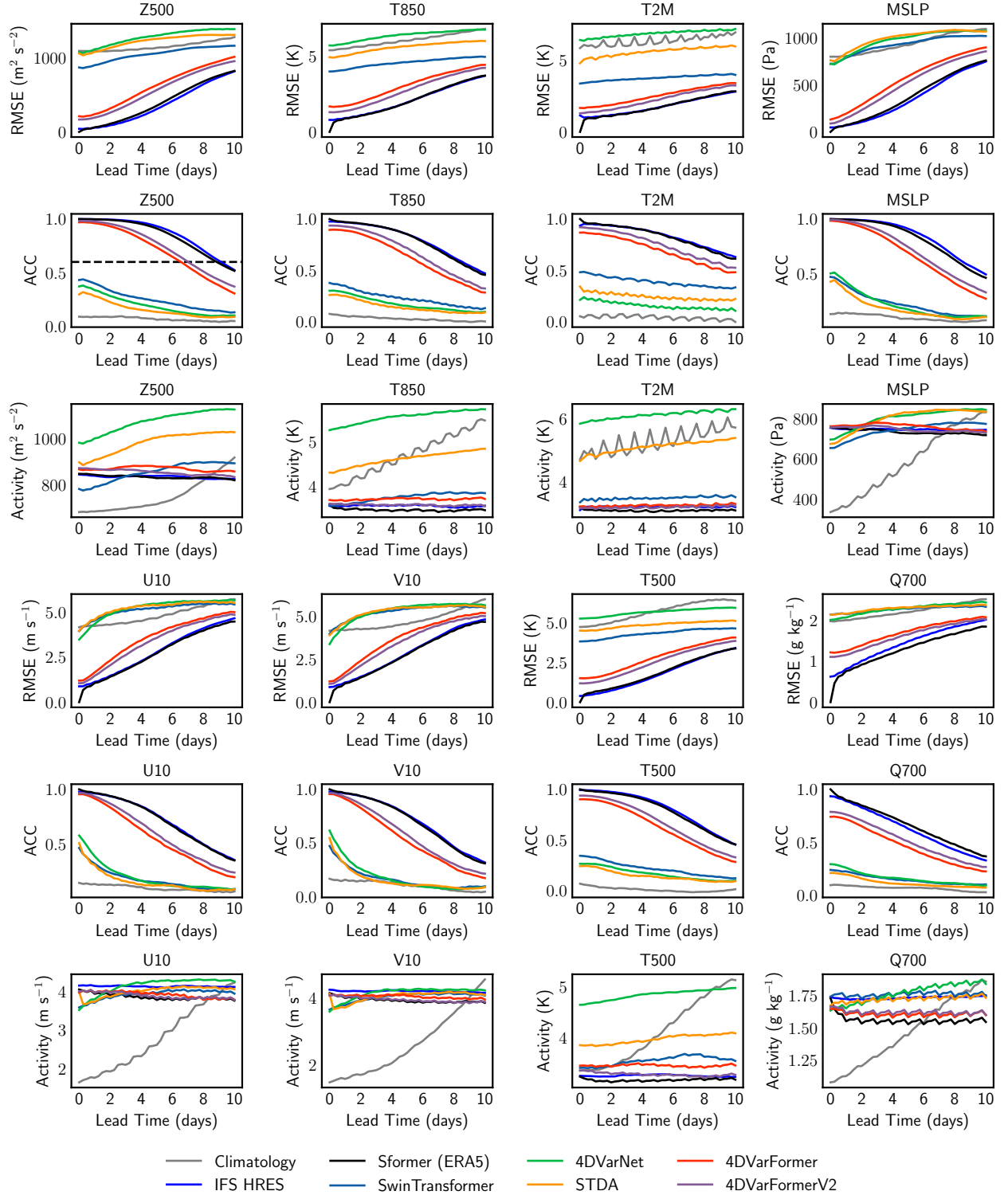


Figure 7: **RMSE, ACC, and Activity metrics of baselines for 10-day medium-range predictions initialized by the analysis fields generated by assimilating real-world observations.** The analysis fields produced by the DA models serve as the initial fields for initializing the medium-range prediction. The results are color-coded as follows: predictions initialized by climatology in gray, operational predictions of IFS HRES in dark blue, predictions initialized by ERA5, SwinTransformer, 4DVarNet, STDA, 4DVarFormer, and 4DVarFormerV2 are shown in black, light blue, green, yellow, red, and purple separately. All metrics are computed against ERA5. Each subplot represents a single variable, as indicated in the subplot titles.

details regarding the EDA methods utilized in this study, please refer to Section 4.5. In this section, we test the EDA in both OSSE and OSE configurations, respectively.

Figure 8 shows the annual metrics of the analysis fields generated by OSSE DA cycles using ensemble methods. Each subplot corresponds to a variable and skill (y-axis) is plotted at 12-hour steps over 365-day horizons (x-axis). Rows 1 and 5 show RMSE, rows 2 and 6 show Bias, rows 3 and 7 show CRPS, while rows 4 and 8 show SSR. The original data is represented with reduced opacity to enhance clarity, while solid lines depict values smoothed using an EMA with an 11-point window. The results indicate that 4DVarFormerV2 outperforms other baselines for our 8 headline variables throughout the one-year DA cycle.

Compared to Figure 2, the RMSE of Z500 produced by the ensemble mean of 4DVarNet is higher, with errors accumulating more rapidly. This suggests that the simple strategy used here may have a detrimental impact on 4DVarNet’s performance. This is further evidenced by the SSR, which experiences a significant increase throughout the one-year assimilation cycle for 4DVarNet, indicating a rapid growth of overdispersion within its ensemble. Conversely, all other baseline methods show a decrease in RMSE. Notably, the SSR ratio for Z500 in 4DVarFormerV2 remains consistent at around 0.6 over the year, demonstrating no increase in dispersion. This stability highlights 4DVarFormerV2’s ability to achieve a relatively stable EDA.

As illustrated in Figure 9, the results obtained under the OSE configuration are closely consistent with those of the OSSE. The RMSE of ensemble means for each DA baseline are lower than the deterministic result, except 4DVarNet. Notably, 4DVarFormerV2 outperforms the other methods in terms of RMSE and CRPS. However, 4DVarFormerV2 exhibits lower SSR metrics compared to both SwinTransformer and STDA across several variables. This indicates that the dispersion of the ensemble members produced by 4DVarFormerV2 under the current ensemble strategy is insufficient.

Figures S11 and S12 present the results of medium-range forecasts initialized by the ensemble means generated by each DA baseline. The performance of each model demonstrates an improvement relative to forecasts derived from deterministic DA methods. In particular, compared to the deterministic results, the Z500 ACC of the forecasts initialized by the ensemble mean of SwinTransformer exceeds 0.6 within the first 2 days, suggesting that EDA significantly enhances the overall performance of AI-based DA. Future research should investigate the integration of AI-based DA with traditional EDA to enhance the operational capabilities of end-to-end weather forecasting systems.

### 3 Discussion

The rapid advancement of LWMs has sparked interest in employing these models to create data-driven end-to-end weather forecasting systems. Currently, LWMs rely on the analysis or reanalysis fields generated by NWP systems as inputs for their forecasts. This reliance makes it difficult for them to operate as self-consistent, stand-alone systems. Recent research has focused on developing data-driven DA models. Nevertheless, a standardized benchmark for impartially evaluating these methods is lacking. To promote the advancement of data-driven end-to-end weather forecasting, we have utilized the ERA5 reanalysis alongside prepbufr observations from the GDAS to establish DABench. This benchmark aims to enhance our understanding of the characteristics of each data-driven DA model. Additionally, we have presented the Sformer prediction model, as well as OSSE and OSE configurations, to enable researchers to assess the performance of their proposed DA models fairly. Additionally, we present a comprehensive comparison of open-source DA models. Furthermore, we provide an update to the recently released three-dimensional multivariate initial field estimation model, 4DVarFormer, resulting in an enhanced version termed 4DVarFormerV2. Compared to existing DA baselines, 4DVarFormerV2 has shown superior robustness and precision in OSSE and OSE tests, achieving a stable and skillful DA cycle for more than a year. Notably, when assimilating GDAS prepbufr observations, 4DVarFormerV2 has successfully initialized Sformer to produce skillful forecasts with lead times of up to 7 days. This result theoretically reinforces the feasibility of developing an operational end-to-end weather forecasting system.

An important caveat of this study is that it specifically focuses on fully data-driven DA models and only compares medium-range forecasting results within a deterministic framework. It should be noted that there is potential for further research in the use of LWMs as surrogate models for conventional DA methods such as 4DVar and the ensemble Kalman filter (EnKF) [36]. Exploring the integration of LWMs into these conventional methods would enable a more comprehensive comparison between purely data-driven DA approaches and hybrid methodologies. Although the evaluation of this study indicates that 4DVarFormerV2 yields better results in ensemble assessments, future research should also assess the performance of ensemble forecasts generated from ensemble members derived from the EDA process. This is particularly important given the highly nonlinear nature of atmospheric dynamics [4].

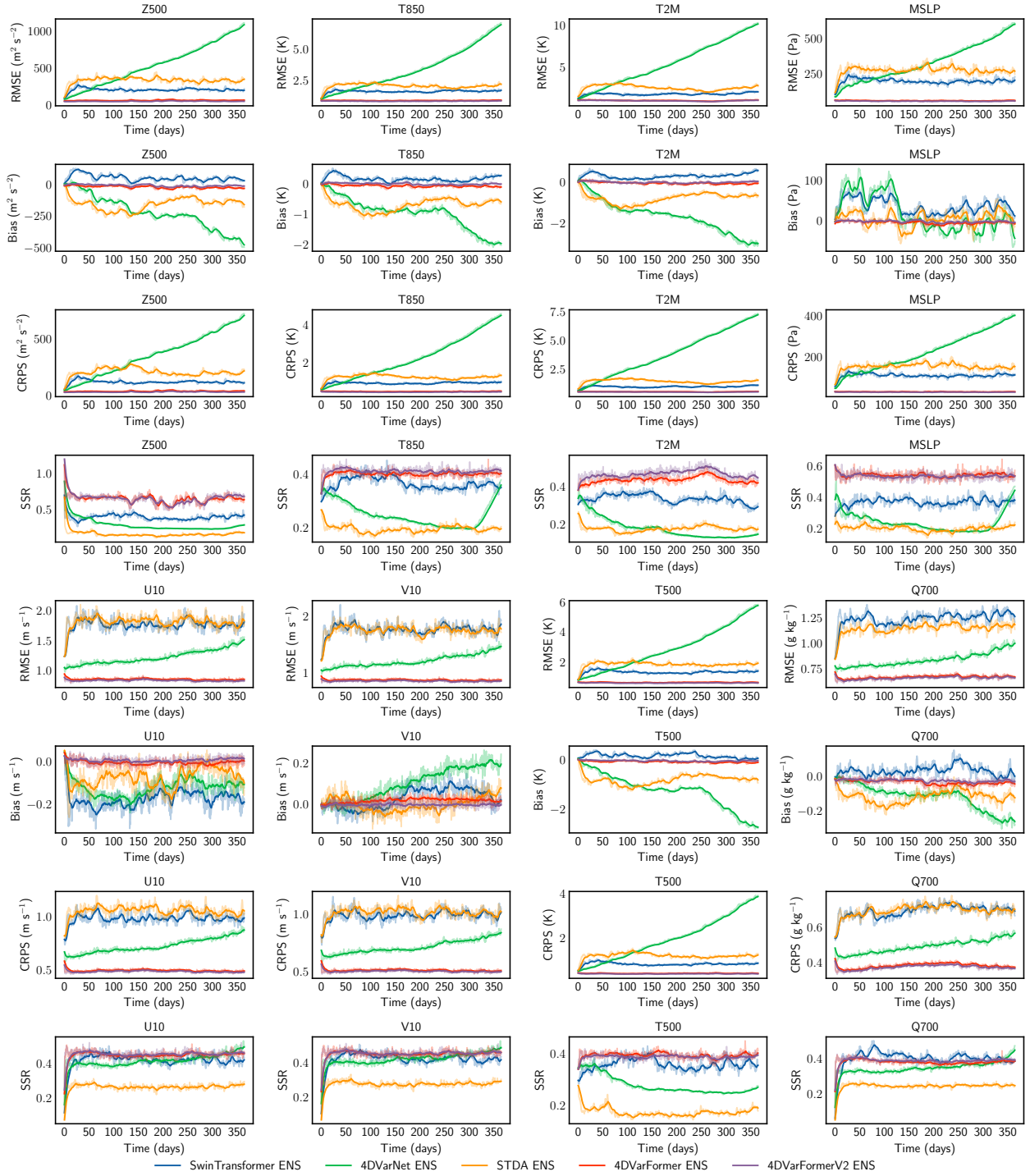


Figure 8: **RMSE, Bias, CRPS, and Spread metrics of baselines over a one-year ensemble DA cycle under the OSSE configuration.** The RMSEs for the analysis fields in 2023 are displayed in odd-numbered rows, while the corresponding Bias metrics are displayed in even-numbered rows. The results are color-coded as follows: the SwinTransformer model in blue, the 4DVarNet model in green, the STDA model in yellow, the 4DVarFormer model in red, and the 4DVarFormerV2 model in purple. These calculations are done for each day of the year at 00:00 UTC and 12:00 UTC. Both RMSE and Bias are computed against ERA5. Each subplot represents a single variable, as indicated in the subplot titles.

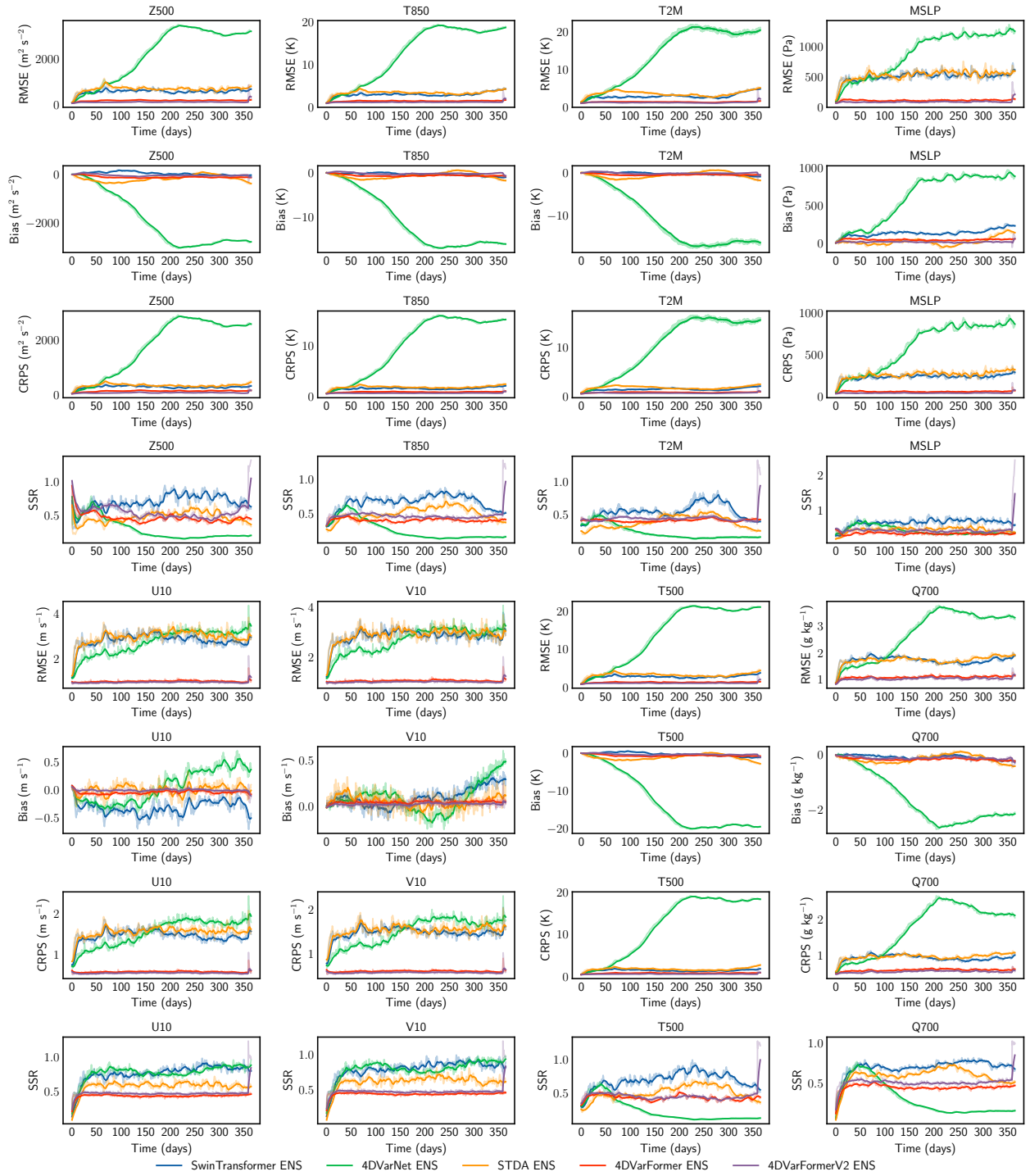


Figure 9: **RMSE, Bias, CRPS, and Spread metrics of baselines over a one-year ensemble DA cycle under the OSE configuration.** The RMSEs for the analysis fields in 2023 are displayed in odd-numbered rows, while the corresponding Bias metrics are displayed in even-numbered rows. The results are color-coded as follows: the SwinTransformer model in blue, the 4DVarNet model in green, the STDA model in yellow, the 4DVarFormer model in red, and the 4DVarFormerV2 model in purple. These calculations are done for each day of the year at 00:00 UTC and 12:00 UTC. Both RMSE and Bias are computed against ERA5. Each subplot represents a single variable, as indicated in the subplot titles.

Another caveat is that we have not considered the assimilation of raw satellite observations, which serve as the primary source for operationalized NWP systems [37]. Our benchmark relies exclusively on GDAS prepbufr conventional observations, while the DA system of IFS utilizes a diverse range of global satellite observations [37]. Therefore, there remains a performance gap when compared to the IFS HRES. Notably, the current results are impressive, given that our model relies solely on GDAS prepbufr observations. A potential solution to enhance performance would be to fine-tune the forecasting model using analysis fields generated by the DA model as initial conditions. Future research should focus on integrating satellite observations to develop a more comprehensive DA model and to create an end-to-end weather prediction system that approaches operational capabilities.

The spatial resolution of 1.40625 degrees in the benchmark proposed here is sufficient for research purposes, but it is indeed insufficient for operational weather forecasting systems. A higher spatial resolution, such as 0.25 degrees or even 0.1 degrees, would be more appropriate for operational purposes [38]. However, it is important to note that increasing the spatial resolution comes with certain challenges. A higher resolution requires a significant increase in data storage and computational costs. This means that more efficient data storage solutions and powerful computing systems would need to be employed. Despite the challenges, investing in improved spatial resolution is essential to achieve more accurate and reliable weather predictions in the future.

We invite the meteorological and AI communities to participate in the development of novel data-driven DA models to accelerate the development of data-driven end-to-end weather forecasting systems. Regarding future research directions, one potential avenue is exploring the training of generative models [39, 19] for DA using sparse and noisy observations as conditions. Furthermore, incorporating uncertainty estimates into the DA models to account for the uncertainties in the observations and background fields is essential. Additionally, it investigates how to combine generative models with existing DA techniques to develop hybrid approaches that leverage the advantages of both data-driven and physics-based methods.

The benchmark established here, along with the success of the 4DVarFormerV2 model in assimilating real-world observations, represents a key advance in end-to-end weather forecasting. This progress holds significant promise for accelerating the development of operational data-driven end-to-end weather forecasting systems. Importantly, our goal is not to replace traditional NWP systems. These systems, refined over decades and rigorously evaluated in diverse real-world contexts, remain invaluable for operational weather forecasting and for providing high-quality datasets for AI. Rather, our findings provide compelling evidence that data-driven weather forecasting systems can effectively address the complexities inherent in real-world forecasting by autonomously assimilating observations. In the future, advances in AI-based DA models are expected to be facilitated by our DABench framework. This enhancement will aid in the development of data-driven end-to-end weather forecasting systems, which will serve as significant complements to NWP systems.

## 4 Materials and Methods

### 4.1 General problem definition

This study considers a weather system that can be represented as follows:

$$\mathbf{x}(t_k) = \mathcal{M}_{t_{k-1} \rightarrow t_k}(\mathbf{x}(t_{k-1})), \quad (1)$$

where  $\mathbf{x}(t_k) \in \mathbb{R}^m$  denotes the system state at the  $t_k$  moment, and  $m$  denotes the system space’s dimension.  $\mathcal{M}_{t_{k-1} \rightarrow t_k} : \mathbb{R}^m \mapsto \mathbb{R}^m$  corresponds to the real-world weather system, which maps the system state at the  $t_{k-1}$  moment into the state at the  $t_k$  moment. This study employs a neural network denoted as  $\mathcal{N}^{\mathcal{M}} : \mathbb{R}^m \mapsto \mathbb{R}^m$  to simulate this system, which is trained on the ERA5 dataset. In discrete time, the observations  $\mathbf{y}(t_k)$  can be denoted as follows:

$$\mathbf{y}(t_k) = \mathcal{H}(\mathbf{x}(t_k)) + \varepsilon^o(t_k), \quad (2)$$

where  $\mathcal{H} : \mathbb{R}^m \mapsto \mathbb{R}^n$  denotes the observation operator and  $n$  denotes the observation space’s dimension. The observation operator  $\mathcal{H}$  is utilized to observe a set of local points from the whole system. The observation error is expressed as a system-independent random error  $\varepsilon^o(t_k)$ , mainly comprising instrumentation and representation errors. Assuming that the observation errors follow a Gaussian distribution, *i.e.*,  $\varepsilon^o \sim \mathcal{N}(0, \mathbf{R})$ , where  $\mathbf{R}$  denotes the observation error covariance matrix [40, 41]. The background field often comes from short-range prediction and is defined as follows:

$$\mathbf{x}^b(t_k) = \mathcal{N}_{t_{k-1} \rightarrow t_k}^{\mathcal{M}}(\mathbf{x}^a(t_{k-1})), \quad (3)$$

where  $\mathbf{x}^a(t_{k-1})$ , called the “analysis field”, is obtained from a DA method.



In the Bayesian formulation, the initial field is estimated as the posterior distribution  $p(\mathbf{x}|\mathbf{y})$  of the unknown state  $\mathbf{x}$  conditioned on the observation  $\mathbf{y}$ , which can be obtained using Bayes’ rule as follows:

$$p(\mathbf{x}|\mathbf{y}) = \frac{p(\mathbf{x}, \mathbf{y})}{p(\mathbf{y})} = \frac{p(\mathbf{y}|\mathbf{x})p(\mathbf{x})}{p(\mathbf{y})}, \quad (4)$$

where  $p(\mathbf{y})$  is denoted as the marginal probability,  $p(\mathbf{x}|\mathbf{y})$  is the posterior probability. To better understand fundamental concepts and conventional DA methods, please refer to [42].

The AI-based DA task aims to develop a neural network that utilizes background fields and observations to generate accurate initial fields. In NWP systems, predictions typically occur daily at 0:00 and 12:00 UTC, limiting the observations available for assimilation in a short-term timeframe (e.g.,  $\geq 00 : 00$  and  $< 12 : 00$  UTC). The AI-based DA model  $\mathcal{N}^{DA}$  can be described as follows:

$$\mathcal{N}^{DA}(\mathbf{x}^b(t_0), \mathbf{y}) : \mathbf{x}^b(t_0), \mathbf{y} \mapsto \mathbf{x}^n(t_0), \quad (5)$$

where  $\mathbf{x}_0^n$  denotes the neural network’s assimilation result,  $\mathbf{y}$  describes the observations in the DAW, and the goal is to make the neural network’s output to approach the true system state  $\mathbf{x}_0^t$  at the initial time  $t_0$ , i.e.,  $(\|\mathbf{x}_0^n - \mathbf{x}_0^t\| \sim 0)$ .

## 4.2 Datasets

Table 1: List of variables contained in the benchmark ground truth dataset. All fields have dimensional  $lat \times lon \times level$ . The number of vertical levels for upper-air variables is given in the table while the level of surface variables and constants is 1.

Upper-air variables (Short name & Unit)	Levels	Surface variables/Constants (Short name & Unit)
Geopotential (Z & $m^2s^{-2}$ )	9	2m_temperature (T2M & K)
Temperature (T & K)	9	10m_u_component_of_wind (U10 & $ms^{-1}$ )
Specific_humidity (Q & $kgkg^{-1}$ )	9	10m_v_component_of_wind (V10 & $ms^{-1}$ )
u_component_of_wind (U & $ms^{-1}$ )	9	mean_sea_level_pressure (MSLP & Pa)
v_component_of_wind (V & $ms^{-1}$ )	9	land_binary_mask (lsm & 0/1)
		Orography (orography & m)

**Ground truth:** Because the reanalysis dataset offers the most accurate historical weather state estimate at each time and location. We utilized the ERA5 dataset [43] as the ground truth for training and testing the DA models. We chose hourly data ranging from 2010 to 2023 and conducted spatial interpolation from a  $0.25^\circ$  latitude/longitude grid ( $721 \times 1440$  grid points) to a  $1.40625^\circ$  latitude/longitude grid ( $128 \times 256$  grid points) following the data construction methodology utilized in [28]. This approach reduces the I/O and memory load for model training. The interpolation was performed utilizing the bilinear interpolation algorithm in the xESMF Python library [44]. Additionally, we selected 9 vertical levels in the upper air, including 50, 200, 250, 300, 500, 700, 850, 925, and 1000 hPa, which correspond to the pressure levels of the publicly available forecasts on the TIGGE archive (<https://confluence.ecmwf.int/display/TIGGE>). We also focused on surface variables such as the 10m wind field, 2m temperature, and mean sea level pressure. The dataset is detailed in Table 1, and stored in the NetCDF file format. We provide Python scripts to convert it to HDF5 for researchers to use, thus accelerating I/O during training.

**Background field:** The background fields employed for the training and validation of our DA model were derived from a 48-hour forecast based on the ERA5 initialization of Sformer. During the final inference phase, the first background field is also a 48-hour forecast initialized from the ERA5 reanalysis, whereas the background fields in subsequent assimilation forecast cycles are derived from forecasts initialized with analysis fields generated by the DA model as shown in Figure 2. The background fields are saved in the HDF5 file format.

**Simulated observations:** The simulated observations in DABench are generated by adding Gaussian noise into the ERA5 dataset. Specifically, the error standard deviation of the added noise is computed based on the GDAS prepbufr observations compared with ERA5 as the reference. We assume observations are obtained every 3 hours, with observation masked ratios of 90%, 95%, and 99%. The observation locations are randomly distributed at any given time. The observations are stored in HDF5 file format. Please refer to Supplementary Material A for details of the OSSE method and the simulated observation error standard deviations.

**Real-world observations:** The real-world observations utilized in this study comprise the GDAS prepbufr conventional observations, which are obtained from the National Centers for Environmental Prediction (NCEP) Automated Data Processing (ADP) global upper-air and surface weather observations available through the NCAR Research Data Archive (NCAR RDA) [30]. These data primarily consist of ground-based observations and satellite-based wind retrievals. The ground-based observations include land and marine surface reports, aircraft data, as well as radiosonde and pilot balloon observations. The satellite-based retrievals are supplied by the National Environmental Satellite Data and Information Service (NESDIS) and include oceanic wind data derived from the Special Sensor Microwave Imager (SSM/I) and upper wind from Low Earth Orbit (LEO) and Geostationary Orbit (GEO) satellites. We converted the GDAS prepbufr observations into 3-hour intervals and employed nearest-neighbor interpolation to map the data onto a grid aligned with the ground truth, thereby achieving a spatial resolution of 1.40625 degrees. Subsequently, we calculated the RMSE for each observation with ERA5 serving as the reference dataset and defined it as the observation error standard deviation.

### 4.3 Sformer

To fairly validate the DA models to get the impact of the generated analysis fields on the prediction results, we provide the Sformer model for researchers. The success of Pangu-Weather [3] indicates that training models with varying lead times and applying the hierarchical temporal aggregation technique can help reduce error accumulation. Nonetheless, the Pangu-Weather [3] approach involves training separate models for different lead times, leading to expensive training costs. In contrast, the recently published Stormer [45] model showcases the effectiveness of utilizing adaptive layer normalization (adaLN) [46] to incorporate the lead time as a control condition, enabling a unified model to predict various lead times. Consequently, we incorporate adaLN to integrate lead time information, facilitating a single model to execute the hierarchical temporal aggregation methodology proposed by Pangu-Weather [3]. The details of the model architecture and hyper-parameters are shown in the Supplementary Material C.

### 4.4 DA baselines

- **Climatology** The climatology is calculated as the average state from 2010 to 2021.
- **SwinTransformer** As illustrated in Figure S2, we establish SwinTransformer [33] as a straightforward baseline, leveraging its ability to directly learn the mapping from background fields and observations to corresponding reanalysis fields.
- **4DVarNet** We transfer the SOTA 4DVarNet [12] model utilized in the domain of SSH reconstitution to our benchmark. The model architecture diagram is represented in Figure S3. We tuned 4DVarNet’s framework to suit our dataset format and task requirements to facilitate its application to our benchmarks.
- **STDA** As illustrated in Figure S4, we adapt the open-source model recently employed for flow field assimilation [34] to the task of weather forecasting. Specifically, it utilizes the Transformer model to incorporate observations from multiple time points within the DAW to accomplish the DA task.
- **4DVarFormer** As illustrated in Figure S5, 4DVarFormer [18] is a Transformer model that integrates 4DVar a priori knowledge, effectively characterizing the relationships between wind-pressure relationship and temperature-humidity relationship. This model ensures accurate predictions of multivariate, three-dimensional atmospheric fields for the East China region within the OSSE framework. We have adapted it for this benchmark to deal with the global DA task.
- **4DVarFormerV2** As illustrated in Figure S6, To further consider the global and local features of the weather, we upgraded 4DVarFormer by incorporating the attention block used in the SwinTransformer model (Swin Attention), thereby constructing a stronger baseline 4DVarFormerV2.

The baseline models were trained and tested using the dataset described in Section 4.2. The training set consisted of data from 2010 to 2021. The year 2022 data was used as the validation dataset. Finally, the year 2023 data was used to test all models. All models were trained using background fields generated from a 48-hour prediction initialized by ERA5 data. The training process for all models was conducted using four NVIDIA A800 GPUs. Please refer to the Supplementary Material C for details of these models above.

### 4.5 EDA configuration

We generated an 11-member ensemble for the DA cycle. Consistent with the methodology used by ECMWF for ensemble simulations [47], which involves perturbing both initial conditions and model physics, we introduced 10 sets of random Perlin noise [3] into the background field at the beginning of the DA cycle. Additionally, we applied

Monte Carlo dropout (MC dropout) [48] with a dropout rate of 0.2 to perturb the DA and forecasting model parameters. Specifically, each of the 10 perturbations includes a distinct Perlin noise, with the number of noise periods generated along each axis—channel, latitude, and longitude—being 1, 4, and 4, respectively. After the initial DA step, no further perturbations are added to the subsequent background fields, as the system autonomously generates EDA results for each time step.

#### 4.6 Metrics

Our objective is to assess the performance of the DA baselines in accordance with the standard evaluation practices of the NWP systems. Consequently, the benchmark established in this study involves a comprehensive evaluation of a one-year DA cycle and a 10-day medium-range forecast. The DA cycle is executed at 12-hour intervals for assimilations, with a DAW of 12 hours. Specifically, the DA cycle is run for the year 2023 at 00:00 UTC and 12:00 UTC each day, which corresponds to the initialization times for the 10-day forecast conducted by the IFS High-RESolution (HRES), Pangu-Weather [3], GraphCast [4], and FengWu [6]. To evaluate medium-range forecasts, we follow the WeatherBench [28], selecting 50 initial fields at 336-hour intervals for the medium-range forecast experiments. The first initial field at 00:00 UTC is set for January 1, 2023, while the first initial field at 12:00 UTC is on January 8, 2023.

All metrics were computed using float32 precision and reported using the native scale of the variables without normalization. Notably, all metrics are computed using a latitude-weighting factor over grid points due to the non-equal area distribution from the equator towards the north and south poles. Let  $\alpha_j$  be the latitude weighting factor for the latitude at the  $j$ th latitude index, which is defined as

$$\alpha_j = \frac{\cos \text{lat}(j)}{\frac{1}{H} \sum_j^H \cos \text{lat}(\hat{j})}, \quad (6)$$

where  $\text{lat}(j)$  represents the latitude of the  $j$ th grid,  $H$  is the number of latitudes in a given resolution.

**Root Mean Square Error (RMSE)** We evaluate assimilate and forecast skill for a given variable,  $\mathbf{x}$ , using a latitude-weighted Root Mean Square Error (RMSE) [28] given by

$$\text{RMSE} = \frac{1}{|D_{eval}|} \sum_{i \in D_{eval}} \sqrt{\frac{1}{HW} \sum_j^H \sum_k^W \alpha_j (\hat{\mathbf{x}}_{i,j,k} - \mathbf{x}_{i,j,k}^t)^2}, \quad (7)$$

where

- $\hat{\mathbf{x}}$  is the field to be evaluated,
- $\mathbf{x}^t$  is the ERA5 ground truth,
- $i \in D_{eval}$  represent the sample index in the evaluation dataset,
- $j$  represents the latitude coordinate in the grid,
- $k$  represents the longitude coordinate in the grid.

The lower the RMSE represents better results.

**Bias** We also computed the bias for a given variable,  $\mathbf{x}$

$$\text{Bias} = \frac{1}{HW} \sum_j^H \sum_k^W \alpha_j (\hat{\mathbf{x}}_{j,k} - \mathbf{x}_{j,k}^t). \quad (8)$$

The closer the Bias is to 0, the better the results are.

**Anomaly Correlation Coefficient (ACC)** To study skillful forecast lead times, we also calculated the latitude-weighted Anomaly Correlation Coefficient (ACC) [28] according to

$$\text{ACC} = \frac{1}{|D_{eval}|} \sum_{i \in D_{eval}} \frac{\sum_{j,k}^{H,W} \alpha_j (\hat{\mathbf{x}}_{j,k} - C_{j,k}) (\mathbf{x}_{j,k}^t - C_{j,k})}{\sqrt{\left[ \sum_{j,k}^{H,W} \alpha_j (\hat{\mathbf{x}}_{j,k} - C_{j,k})^2 \right] \left[ \sum_{j,k}^{H,W} \alpha_j (\mathbf{x}_{j,k}^t - C_{j,k})^2 \right]}}, \quad (9)$$

where  $C_{j,k}$  denotes the climatological mean for a given variable and the day-of-year containing the validity time. It is calculated referring to GraphCast [4] and FengWu [6]. The climatological mean was computed using ERA5 data between 2010 and 2021. The higher the ACC represents better results.

**Activity** To evaluate the smoothness of the forecasts, we introduce the activity metric according to

$$\text{Activity} = \frac{1}{|D_{eval}|} \sum_{i \in D_{eval}} \sqrt{\frac{1}{HW} \sum_{j,k}^{H,W} \alpha_j \left[ (\hat{\mathbf{x}}_{i,j,k} - \mathbf{x}_{i,j,k}^t) - \frac{1}{HW} \sum_{j,k}^{H,W} \alpha_j (\hat{\mathbf{x}}_{i,j,k} - \mathbf{x}_{i,j,k}^t) \right]^2}. \quad (10)$$

The lower the forecast activity the smoother the forecast.

**Continuous Ranked Probability Score (CRPS)** To assess the divergence of AI-based DA methods in our simple ensemble method, we evaluated the Continuous Ranked Probability Score (CRPS) of DA baselines in our EDA experiments. The CRPS was computed using the following equation:

$$\text{CRPS} = \int_{-\infty}^{\infty} [F(\hat{\mathbf{x}}_{j,k}) - \mathcal{G}(\mathbf{x}_{j,k}^t \leq z)] dz, \quad (11)$$

where  $F(\hat{\mathbf{x}}_{j,k})$  represents the cumulative distribution function (CDF) of the  $\hat{\mathbf{x}}_{j,k}$ , and  $\mathcal{G}$  is an indicator function. The indicator function equals 1 if the statement  $\mathbf{x}_{j,k}^t \leq z$  is true; otherwise takes the value of 0. This study uses the xskillscore Python package to calculate the CRPS metric.

**Spread-Skill Ratio (SSR)** The Spread-Skill Ratio (SSR) is defined as the ratio between the ensemble spread and the RMSE of the ensemble mean, where the spread is calculated by the following equation:

$$\text{Spread} = \sqrt{\frac{1}{HW} \sum_{j,k}^{H,W} \alpha_j \text{var}_m(\mathbf{X}_{j,k})}, \quad (12)$$

with  $\text{var}_m$  being the variance in the ensemble dimension. Thus, we define SSR as follows:

$$\text{SSR} = \frac{\text{Spread}}{\text{RMSE}(\bar{\mathbf{X}})}. \quad (13)$$

Smaller SSR indicates an underdispersive forecast, whereas larger SSR indicates an overdispersive forecast.

## Acknowledgments

The authors extend their gratitude to the ECMWF and NCEP for their significant efforts to store and provide invaluable data, which are crucial for this work and the research community. Additionally, this work was carried out at National Supercomputer Center in Tianjin, and the calculations were performed on Tianhe new generation supercomputer. We would also like to express our appreciation to the research team and service team in the Shanghai Artificial Intelligence Laboratory for the provision of computational resources and infrastructure.

**Funding:** Kaijun Ren was supported by the Science and Technology Innovation Program of Hunan Province (2022RC3070). Xiaoyong Li was supported by the National Natural Science Foundation of China (Grant Nos. 42205161). Boheng Duan was supported by the National Natural Science Foundation of China (Grant Nos. 42275170).

**Author contributions:** K.J.R., L.B., and W.X.W. designed the project. K.J.R., L.B., W.C.N., and B.H.D. managed and oversaw the project. W.X.W. and T.K.Y. performed the model training and evaluation. W.X.W. and T.H. improved the model design. W.X.W., T.K.Y., X.Y.L., and T.H. analyze the experiment results. W.X.W., X.Y.L., and W.C.N. wrote and revised the manuscript.

**Competing interests:** The authors declare that they have no competing interests.

**Data and materials availability:** All data needed to evaluate the conclusions in the paper are present in the paper and/or the Supplementary Materials. The DABench dataset is available at the Baidu Drive. The source code used for the benchmark proposed in this work is available in a Github repository <https://github.com/wuxinwang1997/DABench>. The xskillscore Python package can be accessed from <https://github.com/xarray-contrib/xskillscore/>. The implementation of Perlin noise is based on publicly available from the GitHub repository: <https://github.com/pvigier/perlinnumpy/>.

## References

- [1] Andrew Gettelman, Alan J Geer, Richard M Forbes, Greg R Carmichael, Graham Feingold, Derek J Posselt, Graeme L Stephens, Susan C van den Heever, Adam C Varble, and Paquita Zuidema. The future of earth system prediction: Advances in model-data fusion. *Science advances*, 8(14):eabn3488, 2022.
- [2] Jaideep Pathak, Shashank Subramanian, Peter Harrington, Sanjeev Raja, Ashesh Chattopadhyay, Morteza Mardani, Thorsten Kurth, David Hall, Zongyi Li, Kamyar Azizzadenesheli, et al. Fourcastnet: A global data-driven high-resolution weather model using adaptive fourier neural operators. *arXiv preprint arXiv:2202.11214*, 2022.
- [3] Kaifeng Bi, Lingxi Xie, Hengheng Zhang, Xin Chen, Xiaotao Gu, and Qi Tian. Accurate medium-range global weather forecasting with 3d neural networks. *Nature*, 619(7970):533–538, 2023.
- [4] Remi Lam, Alvaro Sanchez-Gonzalez, Matthew Willson, Peter Wirsberger, Meire Fortunato, Ferran Alet, Suman Ravuri, Timo Ewalds, Zach Eaton-Rosen, Weihua Hu, et al. Learning skillful medium-range global weather forecasting. *Science*, 382(6677):1416–1421, 2023.
- [5] Lei Chen, Xiaohui Zhong, Feng Zhang, Yuan Cheng, Yinghui Xu, Yuan Qi, and Hao Li. Fuxi: A cascade machine learning forecasting system for 15-day global weather forecast. *npj Climate and Atmospheric Science*, 6(1):190, 2023.
- [6] Kang Chen, Tao Han, Junchao Gong, Lei Bai, Fenghua Ling, Jing-Jia Luo, Xi Chen, Leiming Ma, Tianning Zhang, Rui Su, et al. Fengwu: Pushing the skillful global medium-range weather forecast beyond 10 days lead. *arXiv preprint arXiv:2304.02948*, 2023.
- [7] Yi Xiao, Lei Bai, Wei Xue, Kang Chen, Tao Han, and Wanli Ouyang. Fengwu-4dvar: Coupling the data-driven weather forecasting model with 4d variational assimilation. *arXiv preprint arXiv:2312.12455*, 2023.
- [8] Kun Chen, Lei Bai, Fenghua Ling, Peng Ye, Tao Chen, Kang Chen, Tao Han, and Wanli Ouyang. Towards an end-to-end artificial intelligence driven global weather forecasting system. *arXiv preprint arXiv:2312.12462*, 2023.
- [9] Wencong Cheng, Yan Yan, Jiangjiang Xia, Qi Liu, Chang Qu, and Zhigang Wang. The compatibility between the pangu weather forecasting model and meteorological operational data. *arXiv preprint arXiv:2308.04460*, 2023.
- [10] Rosangela Cintra, Haroldo de Campos Velho, and Steven Cocke. Tracking the model: Data assimilation by artificial neural network. In *2016 International Joint Conference on Neural Networks (IJCNN)*, pages 403–410. IEEE, 2016.
- [11] Suraj Pawar, Shady E Ahmed, Omer San, Adil Rasheed, and Ionel M Navon. Long short-term memory embedded nudging schemes for nonlinear data assimilation of geophysical flows. *Physics of Fluids*, 32(7):076606, 2020.
- [12] Ronan Fablet, Bertrand Chapron, Lucas Drumetz, Etienne Mémin, Olivier Pannekoucke, and François Rousseau. Learning variational data assimilation models and solvers. *Journal of Advances in Modeling Earth Systems*, 13(10):e2021MS002572, 2021.
- [13] Pin Wu, Xuting Chang, Wenyan Yuan, Junwu Sun, Wenjie Zhang, Rossella Arcucci, and Yike Guo. Fast data assimilation (fda): Data assimilation by machine learning for faster optimize model state. *Journal of Computational Science*, 51:101323, 2021.
- [14] Michael McCabe and Jed Brown. Learning to assimilate in chaotic dynamical systems. *Advances in neural information processing systems*, 34:12237–12250, 2021.
- [15] Wuxin Wang, Kaijun Ren, Boheng Duan, Junxing Zhu, Xiaoyong Li, Weicheng Ni, Jingze Lu, and Taikang Yuan. A four-dimensional variational constrained neural network-based data assimilation method. *Journal of Advances in Modeling Earth Systems*, 16(1):e2023MS003687, 2024.
- [16] Ronan Fablet, Quentin Febvre, and Bertrand Chapron. Multimodal 4dvarnets for the reconstruction of sea surface dynamics from sst-ssh synergies. *IEEE Transactions on Geoscience and Remote Sensing*, 2023.
- [17] Langwen Huang, Lukas Gianinazzi, Yuejiang Yu, Peter D Dueben, and Torsten Hoefler. Diffda: a diffusion model for weather-scale data assimilation. *arXiv preprint arXiv:2401.05932*, 2024.
- [18] Wuxin Wang, Jinrong Zhang, Qingguo Su, Xingyu Chai, Jingze Lu, Weicheng Ni, Boheng Duan, and Kaijun Ren. Accurate initial field estimation for weather forecasting with a variational constrained neural network. *npj Climate and Atmospheric Science*, 7(1):1–17, 2024.
- [19] Prafulla Dhariwal and Alexander Nichol. Diffusion models beat gans on image synthesis. *Advances in neural information processing systems*, 34:8780–8794, 2021.
- [20] Xiaoze Xu, Xiuyu Sun, Wei Han, Xiaohui Zhong, Lei Chen, and Hao Li. Fuxi-da: A generalized deep learning data assimilation framework for assimilating satellite observations. *arXiv preprint arXiv:2404.08522*, 2024.

- [21] François-Xavier Le Dimet and Olivier Talagrand. Variational algorithms for analysis and assimilation of meteorological observations: theoretical aspects. *Tellus A: Dynamic Meteorology and Oceanography*, 38(2):97–110, 1986.
- [22] A Vaswani. Attention is all you need. *Advances in Neural Information Processing Systems*, 2017.
- [23] Sanita Vetra-Carvalho, Peter Jan Van Leeuwen, Lars Nerger, Alexander Barth, M Umer Altaf, Pierre Brasseur, Paul Kirchgeßner, and Jean-Marie Beckers. State-of-the-art stochastic data assimilation methods for high-dimensional non-gaussian problems. *Tellus A: Dynamic Meteorology and Oceanography*, 70(1):1–43, 2018.
- [24] Ahmed Attia and Adrian Sandu. Dates: a highly extensible data assimilation testing suite v1. 0. *Geoscientific Model Development*, 12(2):629–649, 2019.
- [25] Colin Grudzien, Charlotte Merchant, and Sukhreen Sandhu. Dataassimilationbenchmarks. jl: a data assimilation research framework. *Journal of Open Source Software*, 7(79):4129, 2022.
- [26] Patrick N Raanes, Yumeng Chen, and Colin Grudzien. Dapper: data assimilation with python: a package for experimental research. *Journal of Open Source Software*, 9(94):5150, 2024.
- [27] Jia Deng, Wei Dong, Richard Socher, Li-Jia Li, Kai Li, and Li Fei-Fei. Imagenet: A large-scale hierarchical image database. In *2009 IEEE conference on computer vision and pattern recognition*, pages 248–255. Ieee, 2009.
- [28] Stephan Rasp, Peter D Dueben, Sebastian Scher, Jonathan A Weyn, Soukayna Mouatadid, and Nils Thuerey. Weatherbench: a benchmark data set for data-driven weather forecasting. *Journal of Advances in Modeling Earth Systems*, 12(11):e2020MS002203, 2020.
- [29] Makoto Takamoto, Timothy Praditia, Raphael Leiteritz, Daniel MacKinlay, Francesco Alesiani, Dirk Pflüger, and Mathias Niepert. Pdebench: An extensive benchmark for scientific machine learning. *Advances in Neural Information Processing Systems*, 35:1596–1611, 2022.
- [30] National Centers for Environmental Prediction, National Weather Service, NOAA, U.S. Department of Commerce. Ncep adp global upper air and surface weather observations (prepbuf format), 2008. URL <https://rda.ucar.edu/datasets/dsd337000/>.
- [31] Daryl T Kleist and Kayo Ide. An osse-based evaluation of hybrid variational–ensemble data assimilation for the ncep gfs. part i: System description and 3d-hybrid results. *Monthly Weather Review*, 143(2):433–451, 2015.
- [32] Daryl T Kleist and Kayo Ide. An osse-based evaluation of hybrid variational–ensemble data assimilation for the ncep gfs. part ii: 4denvar and hybrid variants. *Monthly Weather Review*, 143(2):452–470, 2015.
- [33] Ze Liu, Yutong Lin, Yue Cao, Han Hu, Yixuan Wei, Zheng Zhang, Stephen Lin, and Baining Guo. Swin transformer: Hierarchical vision transformer using shifted windows. In *Proceedings of the IEEE/CVF international conference on computer vision*, pages 10012–10022, 2021.
- [34] Yuki Yasuda and Ryo Onishi. Spatio-temporal super-resolution data assimilation (srda) utilizing deep neural networks with domain generalization. *Journal of Advances in Modeling Earth Systems*, 15(11):e2023MS003658, 2023.
- [35] L. Isaksen, Massimo Bonavita, Roberto Buizza, Mike Fisher, J. Haseler, Martin Leutbecher, and Laure Raynaud. Ensemble of data assimilations at ecmwf, 12/2010 2010. URL <https://www.ecmwf.int/node/10125>.
- [36] Geir Evensen et al. *Data assimilation: the ensemble Kalman filter*, volume 2. Springer, 2009.
- [37] ECMWF. *IFS Documentation CY47R1 - Part I: Observations*. Number 1. ECMWF, 2020 2020. doi:10.21957/ftq7iq93j. URL <https://www.ecmwf.int/node/19745>.
- [38] R Owens and Tim Hewson. Ecmwf forecast user guide. Technical report, Reading, 05/2018 2018. URL <https://www.ecmwf.int/node/16559>. <p>Replaces previous editions that were available as PDF documents.</p>
- [39] Tero Karras, Samuli Laine, and Timo Aila. A style-based generator architecture for generative adversarial networks. In *Proceedings of the IEEE/CVF conference on computer vision and pattern recognition*, pages 4401–4410, 2019.
- [40] Marco Frei and Hans R Künsch. Mixture ensemble kalman filters. *Computational Statistics & Data Analysis*, 58: 127–138, 2013.
- [41] M. Bocque, P. N. Raanes, and A. Hannart. Expanding the validity of the ensemble kalman filter without the intrinsic need for inflation. *Nonlinear Processes in Geophysics Discussions*, 2015.
- [42] Alberto Carrassi, Marc Bocquet, Laurent Bertino, and Geir Evensen. Data assimilation in the geosciences: An overview of methods, issues, and perspectives. *Wiley Interdisciplinary Reviews: Climate Change*, 9(5):e535, 2018.
- [43] Hans Hersbach, Bill Bell, Paul Berrisford, Shoji Hirahara, András Horányi, Joaquín Muñoz-Sabater, Julien Nicolas, Carole Peubey, Raluca Radu, Dinand Schepers, et al. The era5 global reanalysis. *Quarterly Journal of the Royal Meteorological Society*, 146(730):1999–2049, 2020.

- [44] Jiawei Zhuang, raphael dussin, David Huard, Pascal Bourgault, Anderson Banihirwe, Stephane Raynaud, Brewster Malevich, Martin Schupfner, Filipe, Sam Levang, Charles Gauthier, André Jüling, Mattia Almansì, RichardScottOZ, RondeauG, Stephan Rasp, Trevor James Smith, Jemma Stachelek, Matthew Plough, Pierre, Ray Bell, Romain Caneill, and Xianxiang Li. pangeo-data/xesmf: v0.8.2, September 2023. URL <https://doi.org/10.5281/zenodo.8356796>.
- [45] Tung Nguyen, Rohan Shah, Hritik Bansal, Troy Arcomano, Sandeep Madireddy, Romit Maulik, Veerabhadra Kotamarthi, Ian Foster, and Aditya Grover. Scaling transformer neural networks for skillful and reliable medium-range weather forecasting. *arXiv preprint arXiv:2312.03876*, 2023.
- [46] Ethan Perez, Florian Strub, Harm De Vries, Vincent Dumoulin, and Aaron Courville. Film: Visual reasoning with a general conditioning layer. In *Proceedings of the AAAI conference on artificial intelligence*, volume 32, 2018.
- [47] Roberto Buizza, M Milleer, and Tim N Palmer. Stochastic representation of model uncertainties in the ecmwf ensemble prediction system. *Quarterly Journal of the Royal Meteorological Society*, 125(560):2887–2908, 1999.
- [48] Yarín Gal and Zoubin Ghahramani. Dropout as a bayesian approximation: Representing model uncertainty in deep learning. In *international conference on machine learning*, pages 1050–1059. PMLR, 2016.
- [49] Andrew Brock, Jeff Donahue, and Karen Simonyan. Large scale gan training for high fidelity natural image synthesis. *arXiv preprint arXiv:1809.11096*, 2018.
- [50] William Peebles and Saining Xie. Scalable diffusion models with transformers. In *Proceedings of the IEEE/CVF International Conference on Computer Vision*, pages 4195–4205, 2023.
- [51] Ilya Loshchilov and Frank Hutter. Decoupled weight decay regularization. *arXiv preprint arXiv:1711.05101*, 2017.
- [52] Adam Paszke, Sam Gross, Francisco Massa, Adam Lerer, James Bradbury, Gregory Chanan, Trevor Killeen, Zeming Lin, Natalia Gimelshein, Luca Antiga, et al. Pytorch: An imperative style, high-performance deep learning library. *Advances in neural information processing systems*, 32, 2019.
- [53] William A Falcon. Pytorch lightning. *GitHub*, 3, 2019.
- [54] Ross Wightman. Pytorch image models. <https://github.com/rwightman/pytorch-image-models>, 2019.
- [55] Charles R Harris, K Jarrod Millman, Stéfan J Van Der Walt, Ralf Gommers, Pauli Virtanen, David Cournapeau, Eric Wieser, Julian Taylor, Sebastian Berg, Nathaniel J Smith, et al. Array programming with numpy. *Nature*, 585(7825):357–362, 2020.
- [56] Stephan Hoyer and Joe Hamman. xarray: Nd labeled arrays and datasets in python. *Journal of Open Research Software*, 5(1):10–10, 2017.
- [57] Andrew Collette, Thomas Kluyver, Thomas A Caswell, James Tocknell, Jerome Kieffer, Aleksandar Jelenak, Anthony Scopatz, Darren Dale, Chen, Thomas VINCENT, Matt Einhorn, payno, juliagarriga, Pierlauro Sciarrelli, Valentin Valls, Satrajit Ghosh, Ulrik Kofoed Pedersen, jakirkham, Martin Raspaud, Cyril Danilevski, Hameer Abbasi, John Readey, Kai Mühlbauer, Andrey Paramonov, Lawrence Chan, V. Armando Solé, jialin, Daniel Hay Guest, Yu Feng, and Mark Kittisopikul. h5py/h5py: 3.7.0, May 2022. URL <https://doi.org/10.5281/zenodo.6575970>.
- [58] Diederik P Kingma and Jimmy Ba. Adam: A method for stochastic optimization. *arXiv preprint arXiv:1412.6980*, 2014.

## Supplementary Material for “A Benchmark for AI-based Weather Data Assimilation”

### A Overview of the simulated observations

An Observing System Simulation Experiment (OSSE) [31, 32] is a recognized method for assessing and validating data assimilation (DA) algorithms in numerical weather prediction (NWP) systems. In a traditional NWP OSSE, an unperturbed run of an NWP model is first conducted to establish a reference state, also known as the ground truth. Simulated observations were then generated by extracting relevant variables from the ground truth and incorporating realistic errors. Subsequently, a DA system utilized these simulated observations to evaluate their impact on the analysis field and predictive performance compared to the ground truth.

This study utilized the WeatherBench [28] configuration, with ERA5 reanalysis as the ground truth. The observations simulated in this investigation adhere to the rules mentioned above. The GDAS prepbufr observations from the year 2010 to 2023 are interpolated onto a 1.40625 degrees grid using the nearest interpolation method. The root mean square error (RMSE) of the observations relative to ERA5 is calculated as the standard deviation ( $\sigma$ ) of the error standard deviation. Then, a random error ( $\varepsilon$ ) following the normal Gaussian distribution ( $\varepsilon \sim \mathcal{N}(\mathbf{0}, \sigma^2 \mathbf{I})$ ) is added to ERA5. Subsequently, mask matrices representing the random distribution of discrete observations are randomly generated at each time step, including 90%, 95%, and 99% masked ratios. The observation errors for each variable that we have counted are shown in Table S1.

Table S1: List of Observation Errors for Each Variable.

Variable	Level	Error (Unit)	Variable	Level	Error (Unit)	Variable	Level	Error (Unit)
Z	50hPa	1211 ( $m^2 s^{-2}$ )	T	50hPa	1.679 (K)	Q	50hPa	0.00023 ( $kgkg^{-1}$ )
Z	200hPa	6257 ( $m^2 s^{-2}$ )	T	200hPa	1.591 (K)	Q	200hPa	0.00032 ( $kgkg^{-1}$ )
Z	250hPa	4980 ( $m^2 s^{-2}$ )	T	250hPa	1.642 (K)	Q	250hPa	0.00051 ( $kgkg^{-1}$ )
Z	300hPa	4190 ( $m^2 s^{-2}$ )	T	300hPa	2.523 (K)	Q	300hPa	0.00058 ( $kgkg^{-1}$ )
Z	500hPa	3345 ( $m^2 s^{-2}$ )	T	500hPa	2.694 (K)	Q	500hPa	0.00067 ( $kgkg^{-1}$ )
Z	700hPa	1628 ( $m^2 s^{-2}$ )	T	700hPa	2.115 (K)	Q	700hPa	0.00126 ( $kgkg^{-1}$ )
Z	850hPa	1200 ( $m^2 s^{-2}$ )	T	850hPa	3.283 (K)	Q	850hPa	0.00141 ( $kgkg^{-1}$ )
Z	925hPa	1516 ( $m^2 s^{-2}$ )	T	925hPa	3.574 (K)	Q	925hPa	0.00158 ( $kgkg^{-1}$ )
Z	1000hPa	2671 ( $m^2 s^{-2}$ )	T	1000hPa	5.828 (K)	Q	1000hPa	0.00270 ( $kgkg^{-1}$ )
U	50hPa	3.025 ( $ms^{-1}$ )	V	50hPa	2.862 ( $ms^{-1}$ )	T2M	surface	3.546 (K)
U	200hPa	3.621 ( $ms^{-1}$ )	V	200hPa	3.243 ( $ms^{-1}$ )	U10	surface	1.421 ( $ms^{-1}$ )
U	250hPa	4.280 ( $ms^{-1}$ )	V	250hPa	3.693 ( $ms^{-1}$ )	V10	surface	1.494 ( $ms^{-1}$ )
U	300hPa	5.035 ( $ms^{-1}$ )	V	300hPa	4.219 ( $ms^{-1}$ )	MSLP	surface	225 (Pa)
U	500hPa	5.781 ( $ms^{-1}$ )	V	500hPa	4.407 ( $ms^{-1}$ )			
U	700hPa	4.631 ( $ms^{-1}$ )	V	700hPa	3.982 ( $ms^{-1}$ )			
U	850hPa	3.413 ( $ms^{-1}$ )	V	850hPa	3.027 ( $ms^{-1}$ )			
U	925hPa	3.635 ( $ms^{-1}$ )	V	925hPa	3.134 ( $ms^{-1}$ )			
U	1000hPa	2.503 ( $ms^{-1}$ )	V	1000hPa	2.769 ( $ms^{-1}$ )			

### B Details of the benchmark dataset: data and code

The DABench dataset is released under a license under a CC BY 4.0 International License. Our code implementation is released under the Apache-2.0 License. The license of any specific baseline methods used in our codebase should be verified on their official repositories. In this section, we highlight some details committed in the main text. This includes information on the data structure and the training/evaluation periods.

#### B.1 Data Structure

To accelerate the input-output (IO) of the AI-based model training process, we provide Python code to transform the interpolated ERA5 data from NetCDF format to hdf5 files. Additionally, we extracted the mean and standard deviation of each variable, as well as the static variables and their corresponding statistics. For the preparation of the background field data, we opted for ERA5 data on a 3-hour interval as the initial field. These initial fields served as inputs to the pre-trained Sformer model for inference, yielding 48-hour prediction results used as the background fields in the dataset.



We provide the Python code for generating the background field using Sformer for researchers. Simulated observations were generated by adding noise, as outlined in Section A, to the respective ERA5 data points. Randomized masks were generated on a 3-hourly interval with 90%, 95%, and 99% mask ratios.

The data can be found here with the following directory structure:

- era5
  - 10m\_u\_component\_of\_wind\_1.40625deg
  - 10m\_v\_component\_of\_wind\_1.40625deg
  - 2m\_temperature\_1.40625deg
  - constants\_1.40625deg
  - geopotential\_1.40625deg
  - mean\_sea\_level\_pressure\_1.40625deg
  - specific\_humidity\_1.40625deg
  - temperature\_1.40625deg
  - u\_component\_of\_wind\_1.40625deg
  - v\_component\_of\_wind\_1.40625deg
- osse
  - obs
    - \* train ["times.npz", "2010\_01.h5", ..., "2021\_12.h5"]
    - \* val ["times.npz", "2022\_01.h5", ..., "2022\_12.h5"]
    - \* test ["times.npz", "2023\_01.h5", ..., "2023\_12.h5"]
  - obsmask
    - \* partial\_0.1
      - train ["times.npz", "2010\_01.h5", ..., "2021\_12.h5"]
      - val ["times.npz", "2022\_01.h5", ..., "2022\_12.h5"]
      - test ["times.npz", "2023\_01.h5", ..., "2023\_12.h5"]
    - \* partial\_0.05
      - train ["times.npz", "2010\_01.h5", ..., "2021\_12.h5"]
      - val ["times.npz", "2022\_01.h5", ..., "2022\_12.h5"]
      - test ["times.npz", "2023\_01.h5", ..., "2023\_12.h5"]
    - \* partial\_0.01
      - train ["times.npz", "2010\_01.h5", ..., "2021\_12.h5"]
      - val ["times.npz", "2022\_01.h5", ..., "2022\_12.h5"]
      - test ["times.npz", "2023\_01.h5", ..., "2023\_12.h5"]
- ose
  - obs
    - \* train ["times.npz", "2010\_01.h5", ..., "2021\_12.h5"]
    - \* val ["times.npz", "2022\_01.h5", ..., "2022\_12.h5"]
    - \* test ["times.npz", "2023\_01.h5", ..., "2023\_12.h5"]
  - obsmask
    - \* train ["times.npz", "2010\_01.h5", ..., "2021\_12.h5"]
    - \* val ["times.npz", "2022\_01.h5", ..., "2022\_12.h5"]
    - \* test ["times.npz", "2023\_01.h5", ..., "2023\_12.h5"]
- climatology ["01.h5", "02.h5", ..., "12.h5"]

## B.2 Code Structure

To facilitate the extension of experiments based on our benchmark, we built the code repository based on this template. Our framework greatly reduces the overhead of AI researchers while allowing all researchers to compare algorithms in a unified pipeline. The code can be found here with the following directory structure:

- configs
  - callbacks

- datamodule
- debug
- experiment
- extras
- hparams\_search
- hydra
- local
- logger
- model
  - \* assimilate
  - \* forecast
- paths
- trainer
- eval.yaml
- train.yaml
- logs
- notebooks
- scripts
  - assimilate: scripts for training DA models
  - forecast: scripts for training weather prediction models
  - evaluate: scripts for evaluating prediction and DA models
- src
  - datamodules
    - \* assimilate
    - \* forecast
  - evaluate
  - models
    - \* assimilate
    - \* forecast
  - tasks
  - utils eval.py train.py
- tests: unit test modules

AI researchers have the opportunity to integrate their own assimilation model into the “models/assimilate” directory and compose a configuration file in “configs/model/assimilate” that corresponds with the provided baselines. This pipeline facilitates researchers in effortlessly training their models. Furthermore, researchers can readily devise code for testing inference in the “evaluate” folder according to their model’s specific logic. This procedure should follow the code of baselines, ensuring a fair comparison between the trained model and the baselines.

## C Detail of our weather prediction model – Sformer

### C.1 Model Architecture

As illustrated in Figure S1(a). The Sformer model takes data from both the upper air and surface as inputs. The former encompasses nine pressure levels, each consisting of five variables, resulting in a volume of  $5 \times 9 \times 128 \times 256$ . In contrast, the latter comprises a volume of  $4 \times 128 \times 256$ . Sformer processes the surface variables and the 5 upper-air variables as distinct modalities, leveraging separate patch embedding layers for each modal. In this context, a two-dimensional convolution with a size of  $4 \times 4$  is utilized to transform the data of each modality into a feature space of  $32 \times 64 \times C$ , where  $C$  represents the embedding dimension set to 128 in this investigation. Ultimately, the final dimension of the combined features amounts to  $32 \times 64 \times 6C$ . Subsequently, the combined feature serves as input to the subsequent SwinTransformer [33] blocks and provides predictions.

The success of Pangu-Weather [3] indicates that training models with varying lead times and applying the hierarchical temporal aggregation technique can help reduce the accumulation of errors. To enable a single model to generate

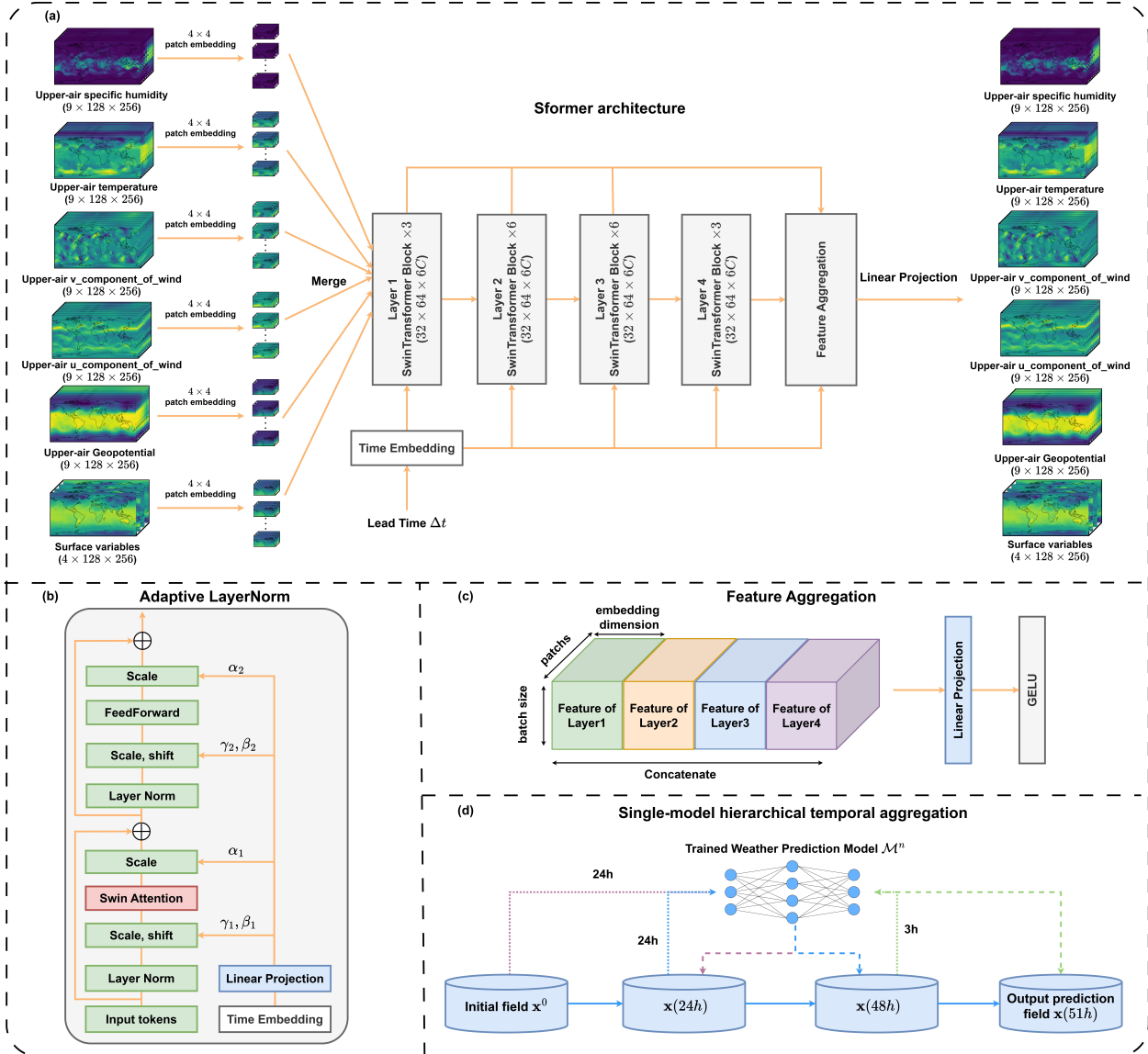


Figure S1: **Details of Sformer's architecture.** (a) The total architecture of Sformer. The model utilizes separate patch embeddings to map different variables into tokens. These tokens are then concatenated along the embedding dimension and passed through four SwinTransformer blocks to obtain the prediction results; (b) The details of the implemented adaptive layer normalization using lead time as the condition; (c) The details of the feature aggregation process in the model; (d) The details of the proposed single-model hierarchical temporal aggregation technique.

predictions with different lead times, we introduce the adaptive layer normalization technique commonly used in generative adversarial networks [49, 39] and diffusion models [19, 50]. It allows the model’s output to be controlled by an additional input representing the lead time. As shown in Figure S1(b), the process involves mapping the lead time to a time embedding using a two-layer Multilayer Perceptron (MLP). This embedding is passed through a linear projection layer. It generates the scale and shift parameters  $(\gamma_1, \beta_1)$  and  $(\gamma_2, \beta_2)$  applied to the outputs of the attention mechanism, as well as the scale parameter  $(\alpha_1, \alpha_2)$  applied to the outputs of the feedforward layer.

As shown in Figure S1(c), we concatenate the normalized features from four different layers along the embedding dimension. Then, an MLP is used to obtain the aggregated features. This operation can combine features from layers at different depths, enhancing the overall representation of the model.

Our proposed algorithm, as shown in Figure S1(d), is the single-model hierarchical time-series aggregation algorithm. It utilizes a greedy algorithm to combine forecasts from a single Sformer model with different lead times. This algorithm enables the efficient inference method introduced by Pangu-Weather [3].

## C.2 Training Details

### C.2.1 Data Normalization

To normalize each variable during the training process, we calculate the mean and standard deviation of each variable in all spatial positions and time points within the training data set. This yields a scalar mean and scalar standard deviation for each variable. Subsequently, throughout the training phase, we subtract the mean value from each variable and then divide it by the standard deviation to achieve data normalization.

### C.2.2 Two-Phase Training

We train Sformer in two phases with the following latitude-weighted  $L_1$ -Loss:

$$\mathcal{L} = \mathbb{E} \left[ \frac{1}{KVHW} \alpha_j \|\hat{\mathbf{x}}(t_k) - \mathbf{x}^t(t_k)\|_1 \right], \quad (14)$$

where  $K$  is the number of rollout steps, which is equal to 1 and 4 in the first and second phases respectively.  $V$  is the number of variables,  $H$  and  $W$  represent the spatial size of a field. In the second phase, we fine-tune the best checkpoint obtained from the first phase.

### C.2.3 Optimization

For the first phase, we train the model for 200 epochs. We optimize the model using AdamW [51] with the learning rate of  $1e - 3$ , parameters  $(\beta_1 = 0.9, \beta_2 = 0.95)$ , and weight decay of  $5e - 5$ . We used a linear warm-up schedule for 10 epochs, followed by a cosine schedule for 190 epochs.

For the second phase, we train the Sformer model for 50 epochs with a constant learning rate of  $3e - 7$ .

We perform early stopping for both phases, where the validation metric is the latitude-weighted  $L_1$  Loss with lead times of 1 day and 4 days for the first and second phases, respectively. We save the best checkpoint for each phase using the same validation metric.

### C.2.4 Software and Hardware being Used

We use PyTorch [52], Pytorch Lightning [53], timm [54], numpy [55], xarray, [56], and h5py [57] for data preparation and model training. We trained Sformer on six 80G A800 GPUs. We use mixed-precision training and distributed data in parallel to reduce memory.

## D Details of the data assimilation baselines

### D.1 SwinTransformer

As illustrated in Figure S2, we establish SwinTransformer [33] as a straightforward baseline, leveraging its ability to directly learn the mapping from background fields and observations to corresponding reanalysis fields. The background field and observations (including the mask matrix) are concatenated along the channel dimension, serving as inputs to the following four SwinTransformer blocks. The model generates the analysis increment and subsequently adds it to the background field, thus producing the analysis field.



Figure S2: **Details of the SwinTransformer baseline's architecture.** The background field and observations (including the mask matrix) are concatenated along the channel dimension, serving as inputs to the model. This model uses the standard SwinTransformer architecture to generate the analysis field.

The baseline example demonstrates a simplified approach to constructing an assimilation model without relying on traditional theories related to assimilation. It is a starting point for understanding the basic input, output, and training processes of building such an AI-based DA model.

## D.2 4DVarNet

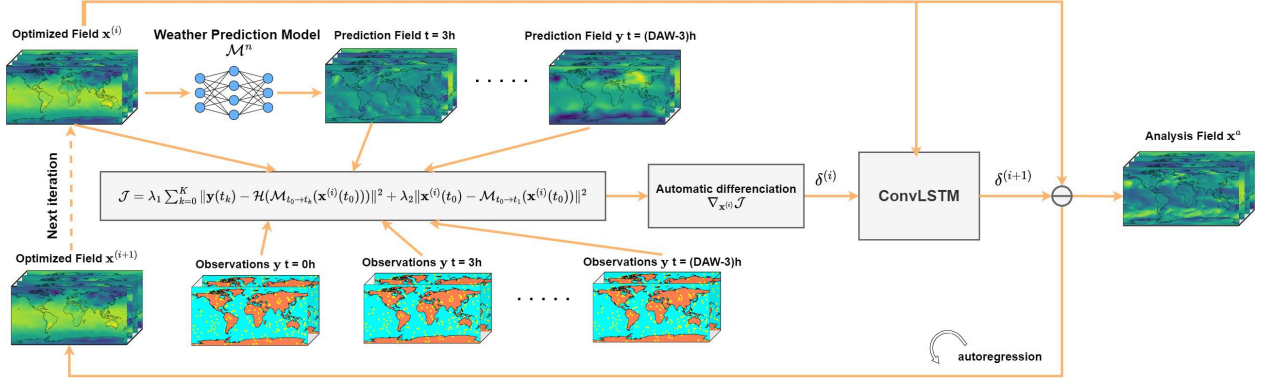


Figure S3: **Model architecture of the tuned 4DVarNet model.** 4DVarNet employs the ConvLSTM for optimizer learning, accelerating the iterative optimization of the simplified 4DVar cost function  $\mathcal{J}$  to provide the final analysis field.

The 4DVarNet model, which relies on the variational DA method, is presented in [12]. It presents a DL approach facilitating the simultaneous training of solvers for modeling dynamical systems and addressing the DA problem. In this study, we implemented the architecture of the 4DVarNet model, as shown in Figure S3. To adapt it to our task and dataset, we fixed the weights of the pre-trained forecast model during the 4DVarNet training process. This ensures that only the solver module for optimizing the 4DVar cost function is trained. The solver module utilizes a Convolutional Long Short-Term Memory (ConvLSTM) model to combine hidden features from historical iteration steps and outputs optimized increments. The 4DVar cost function to be optimized in 4DVarNet model, as described is as follows:

$$\mathcal{J} = \lambda_1 \sum_{k=0}^K \|\mathbf{y}(t_k) - \mathcal{H}(\mathcal{N}_{t_0 \rightarrow t_k}^{\mathcal{M}}(\mathbf{x}^{(i)}(t_0)))\|^2 + \lambda_2 \|\mathbf{x}^{(i)}(t_0) - \mathcal{N}_{t_0 \rightarrow t_1}^{\mathcal{M}}(\mathbf{x}^{(i)}(t_0))\|^2, \quad (15)$$

where  $\mathcal{N}_{t_{k-1} \rightarrow t_k}^{\mathcal{M}}$  denotes the pre-trained weather prediction model Sformer,  $\mathbf{x}^{(i)}(t_0)$  represents the analysis field to be optimized at the  $i$ th iteration,  $\mathbf{y}(t_k)$  denotes the observations at the  $t_k$  moment, and  $\mathcal{H}$  represents the observation operator. In this study,  $\mathcal{H}$  is the mask matrix. Moreover,  $\lambda_1$  and  $\lambda_2$  represent the weight factors of the two components of the cost function.

## D.3 STDA

STDA [34] is a U-Transformer model designed for the estimate of 3D fluid dynamics. Its structural representation is illustrated in Figure S4. It effectively maps the background field and observations within a DAW to a unified latent

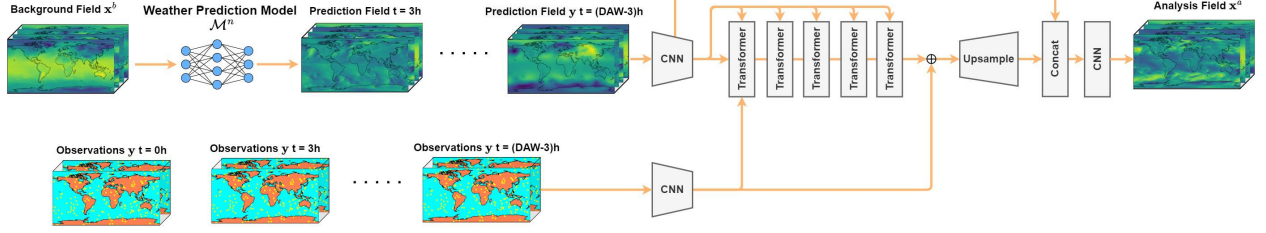


Figure S4: **Model architecture of the tuned STDA model.** STDA employs the U-Transformer to learn the mapping from the background field and observations to the analysis field.

space. This process involves two downsampling blocks constructed by convolutional neural networks. Subsequently, it fuses these two features through a Transformer model and employs upsampling along with skip connections to produce the analysis fields.

#### D.4 4DVarFormer

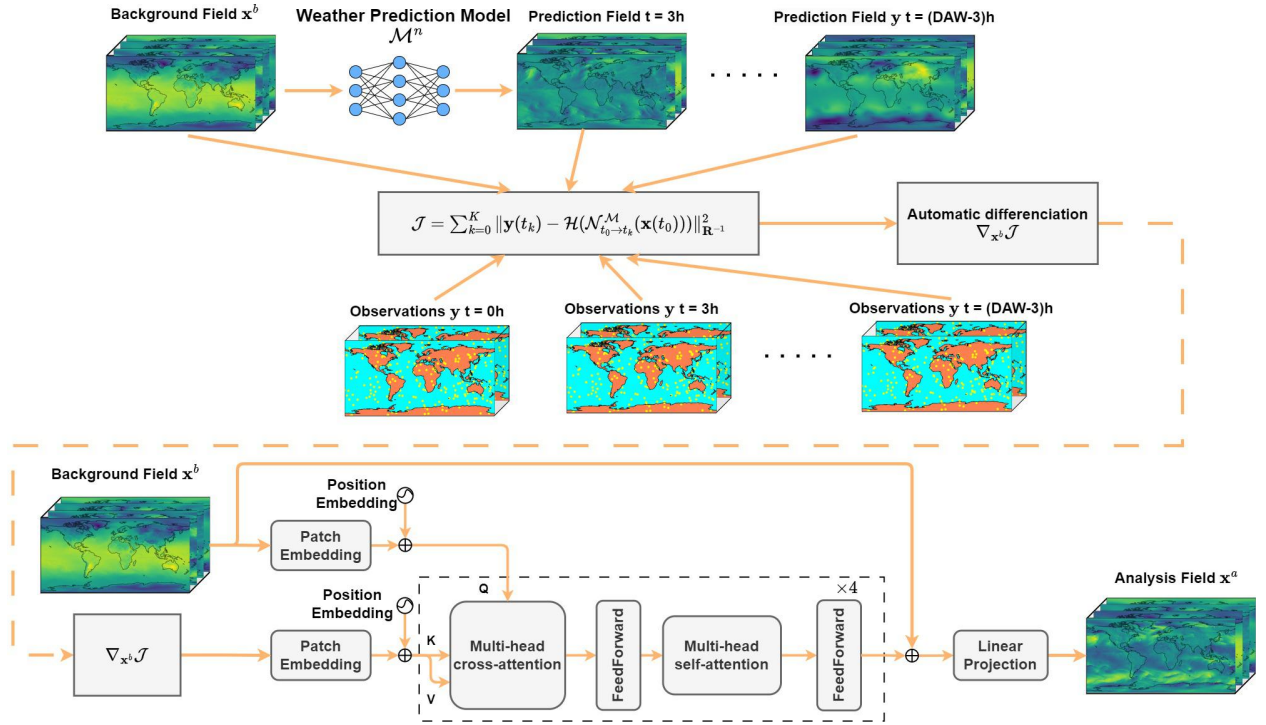


Figure S5: **Model architecture of the 4DVarFormer model.** The 4DVarFormer utilizes the Transformer model to integrate the background field and the gradient of the 4DVar cost function, thereby estimating the accurate analysis field.

4DVarFormer [18] is a model that incorporates 4DVar constraints into an attention-based neural network, eliminating the need for background error covariance statistics and the development of the complex concomitant model. It captures inter-variable relationships, allowing for the assimilation of observed variables to correct unobserved variables. 4DVarFormer’s architecture is illustrated in Figure S5.

The 4DVar cost function used in 4DVarFormer is as follows:

$$\mathcal{J} = \frac{1}{2} \|\mathbf{x}(t_0) - \mathbf{x}^b(t_0)\|_{\mathbf{B}^{-1}}^2 + \frac{1}{2} \sum_{k=0}^K \|\mathbf{y}(t_k) - \mathcal{H}(\mathcal{N}_{t_0 \rightarrow t_k}^{\mathcal{M}}(\mathbf{x}(t_0)))\|_{\mathbf{R}^{-1}}^2. \quad (16)$$

Since our model is non-autoregressive, we only need to input  $\mathbf{x}(t_0) = \mathbf{x}^b(t_0)$  and calculate the derivative. In this context, the first term of the above cost function is equal to 0. Therefore, we can use the following simplified cost



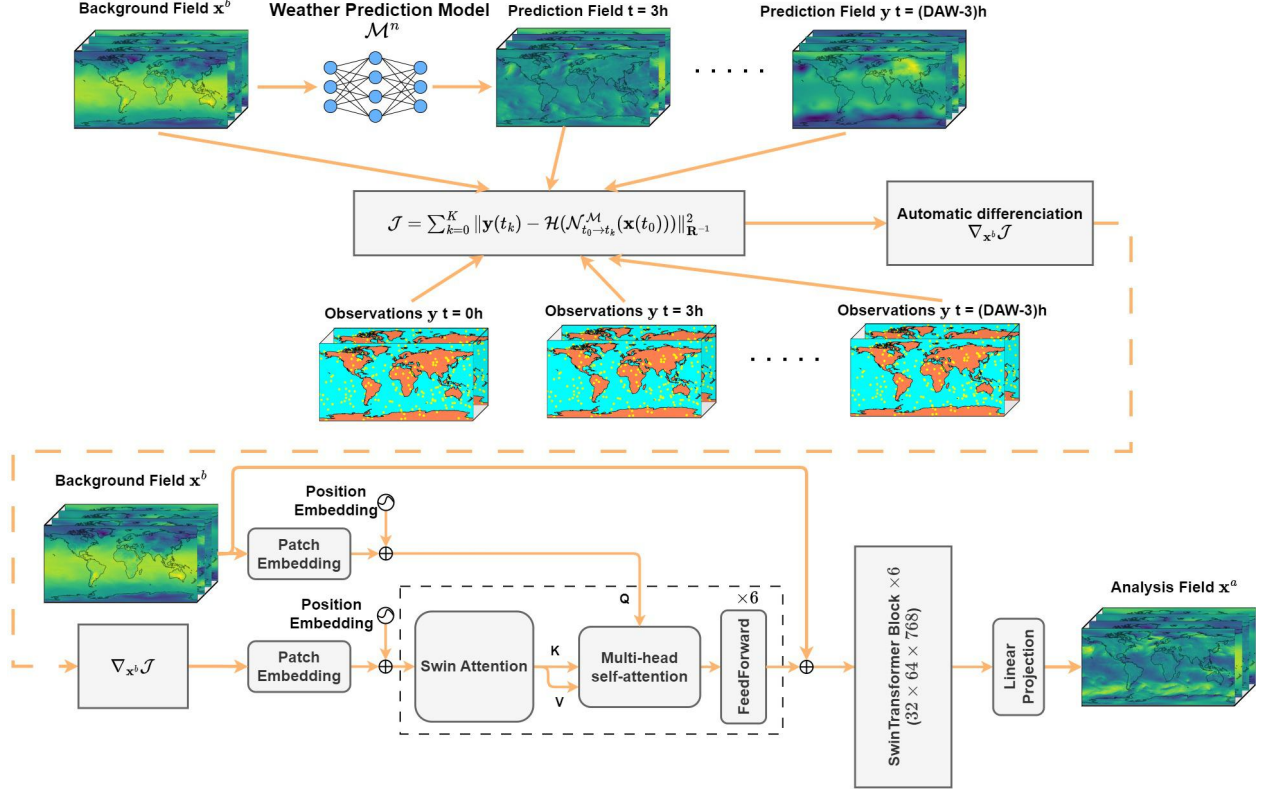


Figure S6: **Model architecture of the 4DVarFormerV2 model.** 4DVarFormerV2 employs Swin Attention to enhance the original 4DVarFormer’s capacity for capturing localized features. Additionally, it incorporates the Swin-Transformer block to construct a decoder that more effectively integrates the latent background field with the analysis increments.

#### D.6.4 Software and Hardware being Used

Please refer to subsection C.2.4.

## E More DA cycle results

### E.1 More details of the OSSE results

To analyze the deterministic DA cycle under OSSE, we selected several key variables (Z500, T2M, T850), the results of which are presented in Table S2. The findings indicate that 4DVarFormerV2 generally outperforms other methods in terms of RMSE when assimilating 90% masked observations. This suggests that 4DVarFormerV2 effectively addresses the assimilation task.

It is important to note that while the climatology and the SwinTransformer exhibit high RMSE, they demonstrate Bias close to 0. This phenomenon is likely attributed to their spatial and seasonally oscillating Bias, which trends toward zero in the yearly time-averaged values. Consequently, the bias does not serve as a direct indicator of the quality of the analysis fields; however, it can aid in discerning the properties of the model.

Figure S7 demonstrates that the SwinTransformer when trained with 90% masked observations, exhibits a significant RMSE and Bias when assimilating observations with a 99% masking ratio. This finding indicates that the robustness of the SwinTransformer is limited, rendering it less effective in handling complex and variable observational scenarios.

Additionally, as illustrated in Figures S8 and S9, 4DVarNet and STDA exhibit similar issues to SwinTransformer. In contrast, Figure S10 demonstrates that 4DVarFormer has a more stable Bias.



Table S2: Comparison of one-year DA cycle performances with different methods under OSSE configuration. We computed the average RMSE, and Bias of the 12-hourly analysis field throughout a year to evaluate the overall performance of the models. The best results in baselines are bolded.

Method	RMSE ↓			Bias		
	Z500 $m^2 s^{-2}$	T850 K	T2M K	Z500 $m^2 s^{-2}$	T850 K	T2M K
Climatology	1081	5.440	6.01	<b>0.589</b>	0.025	0.034
SwinTransformer	435	2.555	2.531	72	0.183	0.431
4DVarNet	317	2.072	3.375	217	-0.131	-0.188
STDA	685	3.622	4.118	479	-1.077	-1.283
4DVarFormer	84	0.878	1.049	-24	<b>-0.0508</b>	-0.087
4DVarFormerV2	<b>64</b>	<b>0.808</b>	<b>0.981</b>	7	0.077	<b>0.076</b>

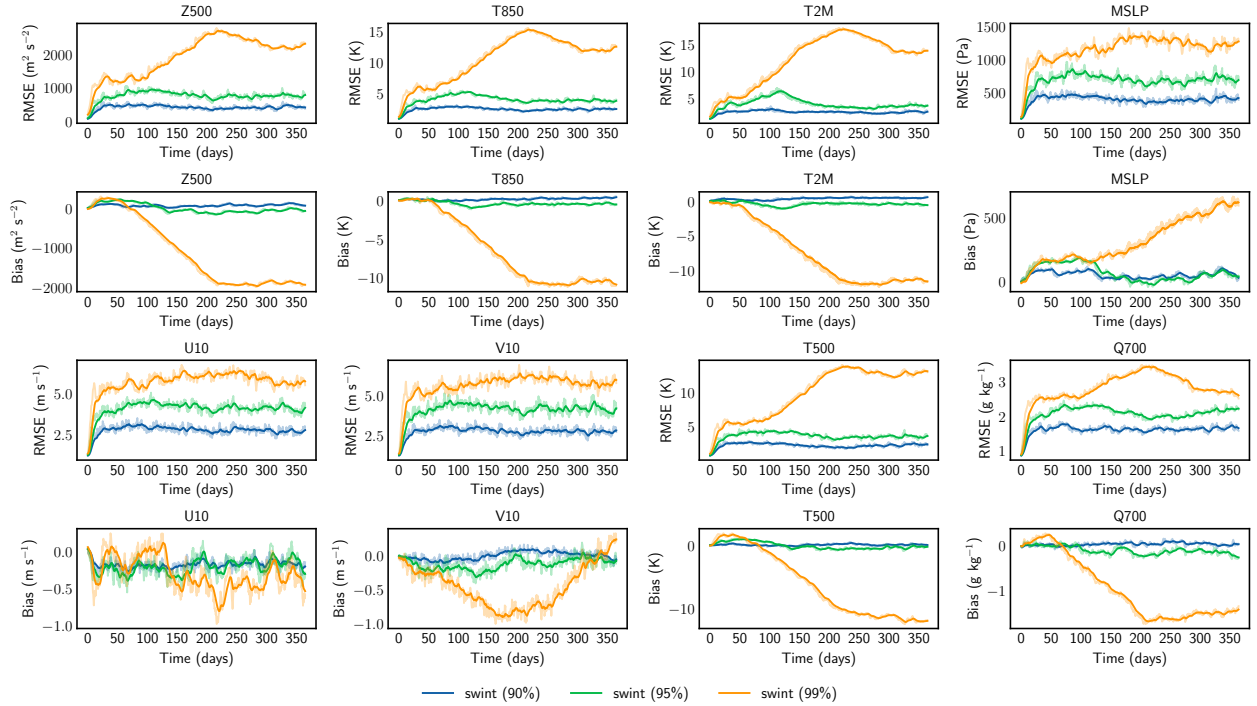


Figure S7: **RMSE and Bias metrics of SwinTransformer over a one-year DA cycle using different observational mask ratios.** The RMSEs for the analysis fields in the year 2023 are displayed in odd-numbered rows, while the corresponding Bias metrics are displayed in even-numbered rows. The results are color-coded as follows: 90% masked results are in blue, 95% masked results are in green, and 99% masked results are in yellow. These calculations are done for each day of the year at 00:00 UTC and 12:00 UTC. Both RMSE and Bias are computed against ERA5. Each subplot represents a single variable, as indicated in the subplot titles.

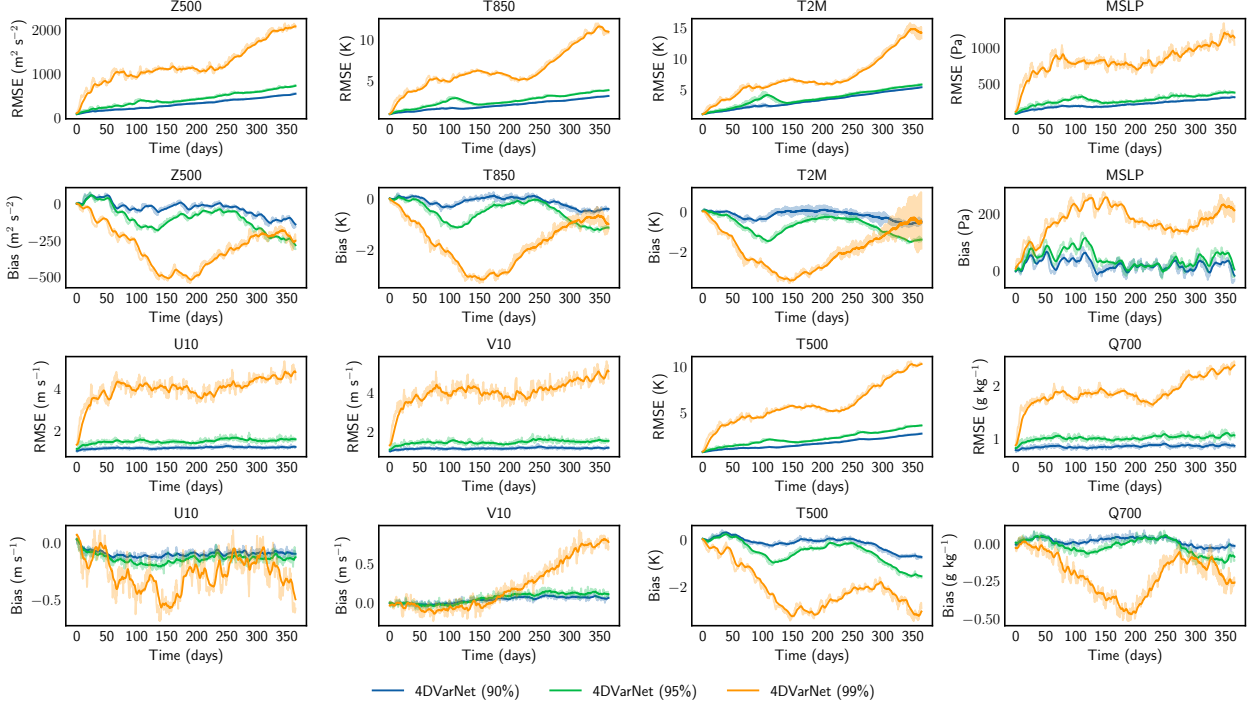


Figure S8: **RMSE and Bias metrics of 4DVarNet over a one-year DA cycle using different observational mask ratios.** The RMSEs for the analysis fields in 2023 are displayed in odd-numbered rows, while the corresponding Bias metrics are displayed in even-numbered rows. The results are color-coded as follows: 90% masked results are in blue, 95% masked results are in green, and 99% masked results are in yellow. These calculations are done for each day of the year at 00:00 UTC and 12:00 UTC. Both RMSE and Bias are computed against ERA5. Each subplot represents a single variable, as indicated in the subplot titles.

## E.2 More details of the OSE results

To analyze the deterministic DA cycle under OSE, we selected several key variables (Z500, T2M, T850) whose results are presented in Table S3. The findings indicate that 4DVarFormerV2 has the lowest RMSE metrics when assimilating real-world observations. This suggests that 4DVarFormerV2 effectively addresses the real-world assimilation task.

Table S3: Comparison of one-year DA cycle performances with different methods under OSE configuration. We computed the average RMSE, and Bias of the 12-hourly analysis field throughout a year to evaluate the overall performance of the models. The best results in baselines are bolded.

Method	RMSE ↓			Bias		
	Z500 $m^2 s^{-2}$	T850 K	T2M K	Z500 $m^2 s^{-2}$	T850 K	T2M K
Climatology	1081	5.440	6.01	<b>0.589</b>	<b>0.025</b>	<b>0.034</b>
SwinTransformer	873	4.045	3.388	21	-0.220	0.084
4DVarNet	1124	6.087	6.890	741	-1.378	-1.192
STDA	1056	4.958	4.831	-239	-0.796	-0.692
4DVarFormer	215	1.701	1.693	-60	-0.502	-0.597
4DVarFormerV2	<b>167</b>	<b>1.309</b>	<b>1.299</b>	68	0.330	0.311

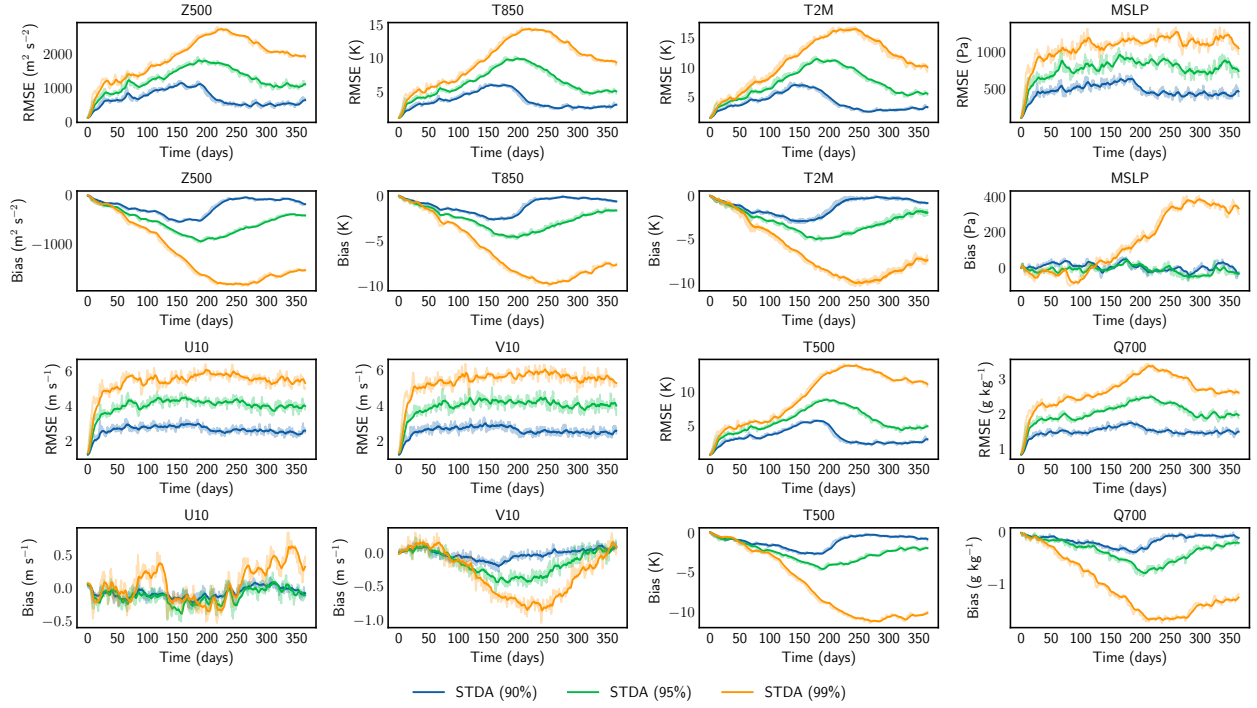


Figure S9: **RMSE and Bias metrics of STDA over a one-year DA cycle using different observational mask ratios.** The RMSEs for the analysis fields in 2023 are displayed in odd-numbered rows, while the corresponding Bias metrics are displayed in even-numbered rows. The results are color-coded as follows: 90% masked results are in blue, 95% masked results are in green, and 99% masked results are in yellow. These calculations are done for each day of the year at 00:00 UTC and 12:00 UTC. Both RMSE and Bias are computed against ERA5. Each subplot represents a single variable, as indicated in the subplot titles.

## F More medium-range forecasting results

The results of the analysis field-driven 10-day medium-range forecasts for each DA baseline in both OSSE and OSE configurations are presented in Tables S4 and S5. We include the results from the IFS HRES and the Sformer model using ERA5 as the initial field as reference values in the first two rows of these tables. Notably, the RMSE and ACC of 4DVarFormerV2 significantly surpass those of the other baselines in both the 90% masked and real-world observation experiments, with this trend being particularly pronounced in the real-world observations experiment. This suggests that 4DVarFormerV2 effectively utilizes extremely sparse conventional observations to initialize accurate forecasts. Furthermore, the similarity between the Activity calculated by the 4DVarFormerV2-driven forecast and that produced by the ERA5-driven Sformer model indicates that the 4DVarFormerV2 effectively captures the spatial structure of the atmosphere. This capability helps mitigate the negative influence of the sparse and noisy observations on the Sformer forecast, which may result in spurious noise.

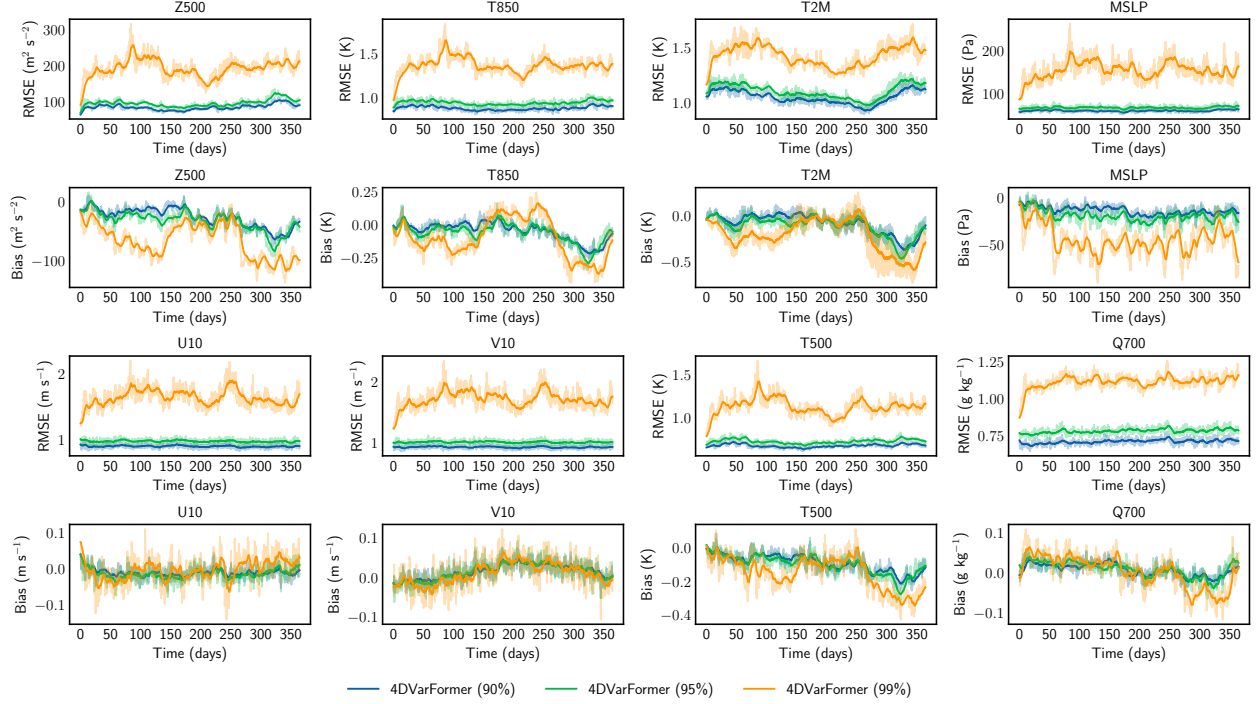


Figure S10: **RMSE and Bias metrics of 4DVarFormer over a one-year DA cycle using different observational mask ratios.** The RMSEs for the analysis fields in 2023 are displayed in odd-numbered rows, while the corresponding Bias metrics are displayed in even-numbered rows. The results are color-coded as follows: 90% masked results are in blue, 95% masked results are in green, and 99% masked results are in yellow. These calculations are done for each day of the year at 00:00 UTC and 12:00 UTC. Both RMSE and Bias are computed against ERA5. Each subplot represents a single variable, as indicated in the subplot titles.

Table S4: Comparison of 10-day medium-range forecasting performances with different methods under OSSE configuration. We computed the average RMSE, ACC, and Activity of the 6-hourly forecast to evaluate the overall performance of the models. The best results in baselines are bolded.

Method	3 / 5 day RMSE ↓			3 / 5 day ACC ↑			3 / 5 day Activity		
	Z500 $m^2s^{-2}$	T850 K	T2M K	Z500	T850	T2M	Z500 $m^2s^{-2}$	T850 K	T2M K
IFS HRES	143/308	1.342/1.969	1.317/1.693	0.986/0.933	0.931/0.851	0.918/0.863	838/840	3.593/3.600	3.216/3.216
Sformer (ERA5)	176/352	1.300/1.929	1.244/1.642	0.978/0.912	0.934/0.852	0.924/0.866	840/830	3.468/3.466	3.086/3.073
Climatology	1101/1131	5.768/6.044	5.973/6.158	0.085/0.061	0.038/0.022	0.035/0.022	698/717	4.334/4.636	4.845/5.016
SwinTransformer	706/859	3.374/3.923	2.907/3.251	0.646/0.490	0.562/0.425	0.612/0.520	827/851	3.572/3.634	3.269/3.306
4DVarNet	429/593	2.505/3.134	3.469/3.749	0.878/0.771	0.785/0.668	0.620/0.556	902/901	3.962/3.996	4.310/4.339
STDA	913/1064	4.597/5.117	4.486/4.807	0.501/0.353	0.407/0.293	0.440/0.382	918/956	4.353/4.467	4.462/4.557
4DVarFormer	220/411	1.465/2.168	1.392/1.815	0.966/0.881	0.917/0.818	0.905/0.837	857/851	3.544/3.556	3.108/3.112
4DVarFormerV2	<b>202/390</b>	<b>1.403/2.080</b>	<b>1.349/1.757</b>	<b>0.972/0.893</b>	<b>0.923/0.831</b>	<b>0.911/0.847</b>	852/846	3.511/3.515	3.091/3.093

Table S5: Comparison of 10-day medium-range forecasting performances with different methods under OSE configuration. We computed the average RMSE, ACC, and Activity of the 6-hourly forecast to evaluate the overall performance of the models. The best results in baselines are bolded.

Method	3 / 5 day RMSE ↓			3 / 5 day ACC ↑			3 / 5 day Activity		
	Z500 $m^2s^{-2}$	T850 K	T2M K	Z500	T850	T2M	Z500 $m^2s^{-2}$	T850 K	T2M K
IFS HRES	143/308	1.342/1.969	1.317/1.693	0.986/0.933	0.931/0.851	0.918/0.863	838/840	3.593/3.600	3.216/3.216
Sformer (ERA5)	176/352	1.300/1.929	1.244/1.642	0.978/0.912	0.934/0.852	0.924/0.866	840/830	3.468/3.466	3.086/3.073
Climatology	1101/1131	5.768/6.044	5.973/6.158	0.085/0.061	0.038/0.022	0.035/0.022	698/717	4.334/4.636	4.845/5.016
SwinTransformer	1004/1131	4.430/6.044	3.640/6.158	0.289/0.236	0.270/0.224	0.418/0.386	839/852	3.714/3.789	3.458/3.474
4DVarNet	1224/1296	6.230/6.486	6.740/6.933	0.239/0.174	0.211/0.154	0.168/0.133	1055/1089	5.479/5.568	6.057/6.155
STDA	1185/1251	5.440/5.685	5.367/5.627	0.179/0.134	0.173/0.130	0.278/0.245	958/1006	4.519/4.630	5.036/5.184
4DVarFormer	417/628	2.332/3.105	2.066/2.502	0.884/0.735	0.800/0.647	0.800/0.710	880/880	3.715/3.735	3.244/3.276
4DVarFormerV2	<b>349/563</b>	<b>1.961/2.740</b>	<b>1.733/2.205</b>	<b>0.918/0.782</b>	<b>0.855/0.717</b>	<b>0.857/0.770</b>	869/854	3.587/3.586	3.180/3.188

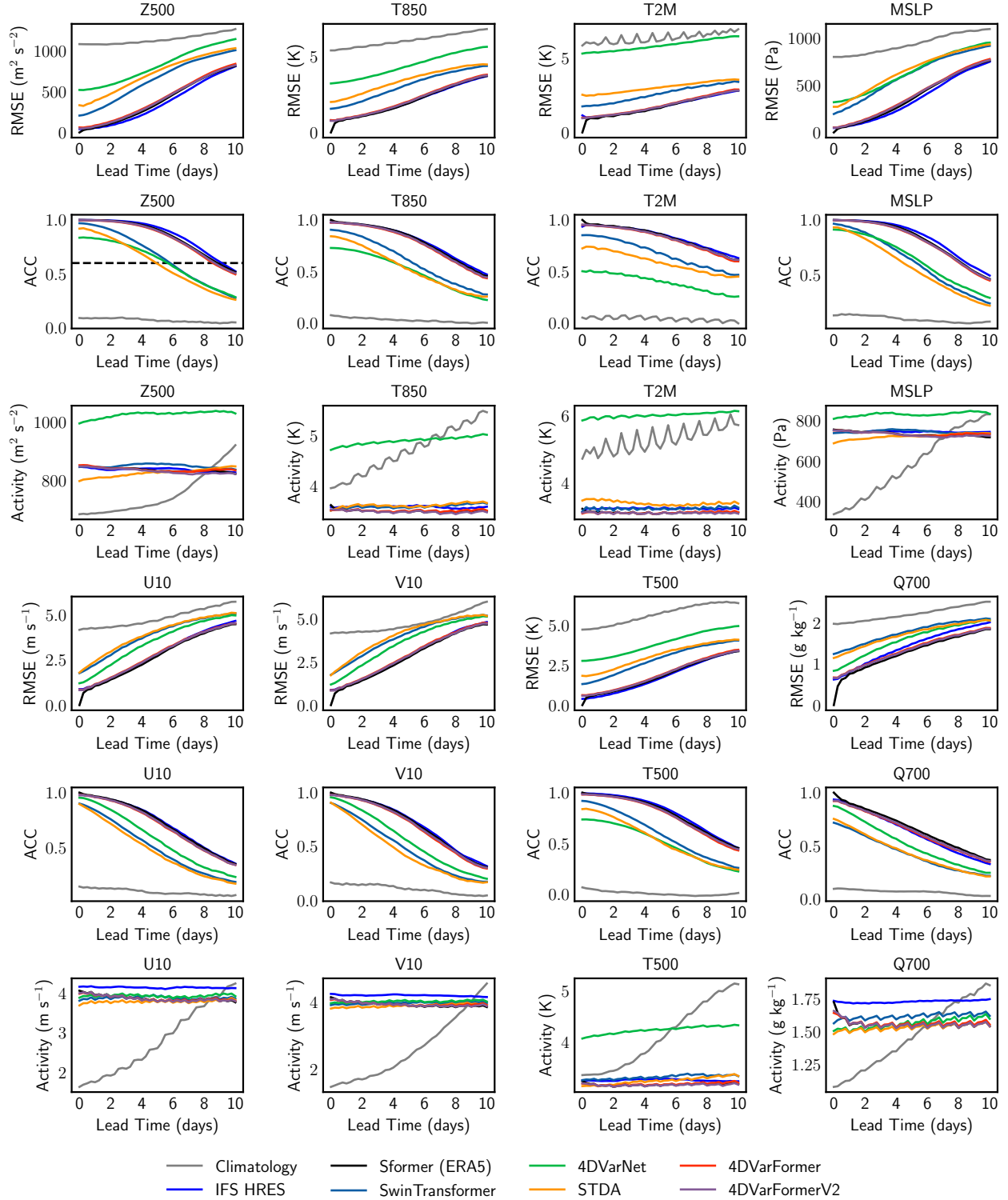


Figure S11: **RMSE, ACC, and Activity metrics of baselines for 10-day medium-range predictions initialized by the analysis fields assimilating 90% masked observations with EDA.** The analysis fields produced by the DA models serve as the initial fields for driving the medium-range predictions. The results are color-coded as follows: predictions initialized by climatology in gray, operational predictions of IFS HRES in dark blue, predictions initialized by ERA5, SwinTransformer, 4DVarNet, STDA, 4DVarFormer, and 4DVarFormerV2 are shown in black, light blue, green, yellow, red, and purple separately. All metrics are computed against ERA5. Each subplot represents a single variable, as indicated in the subplot titles.

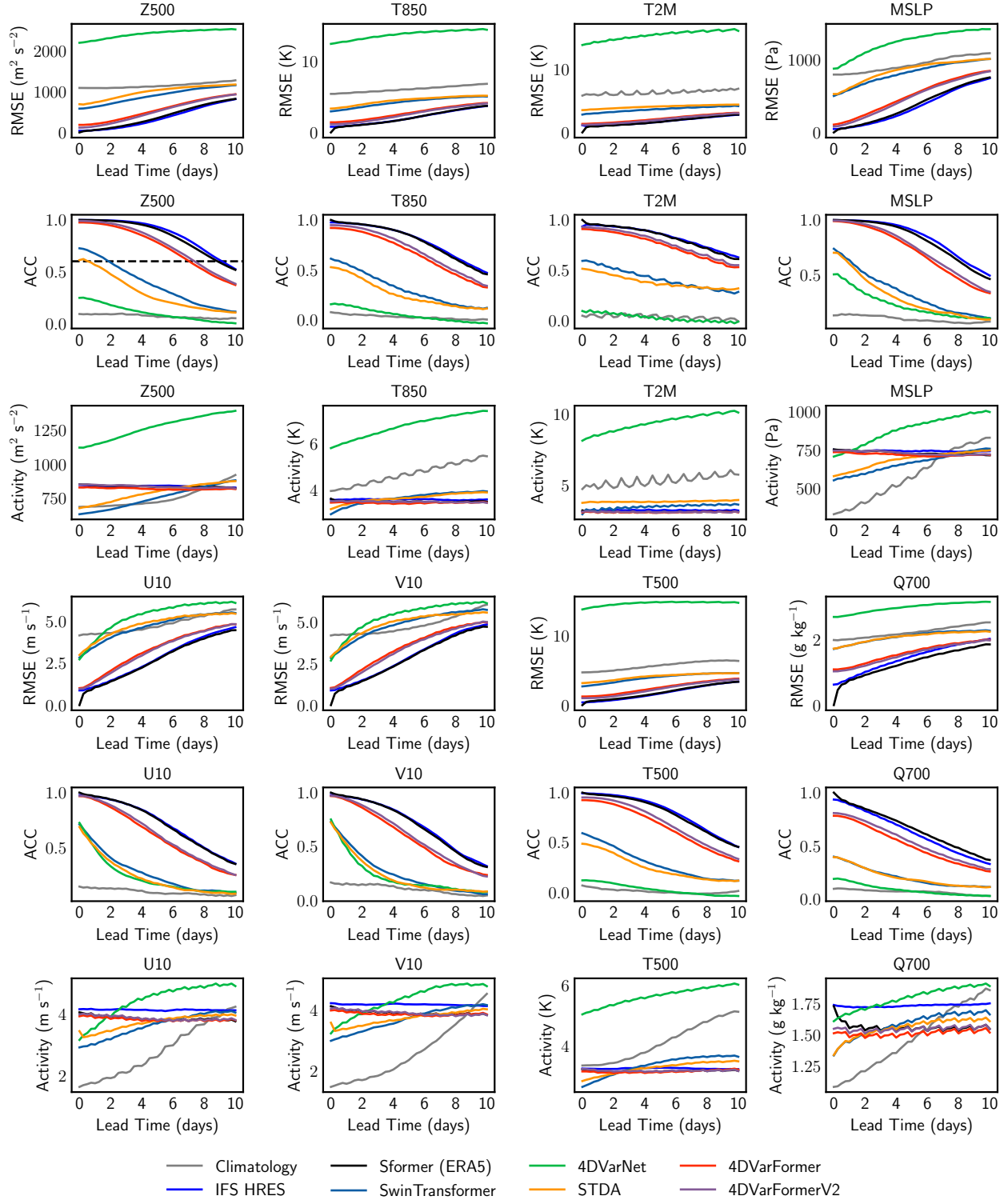


Figure S12: **RMSE, ACC, and Activity metrics of baselines for 10-day medium-range predictions initialized by the analysis fields assimilating real-world observations with EDA.** The analysis fields produced by the DA models serve as the initial fields for driving the medium-range predictions. The results are color-coded as follows: predictions initialized by climatology in gray, operational predictions of IFS HRES in dark blue, predictions initialized by ERA5, SwinTransformer, 4DVarNet, STDA, 4DVarFormer, and 4DVarFormerV2 are shown in black, light blue, green, yellow, red, and purple separately. All metrics are computed against ERA5. Each subplot represents a single variable, as indicated in the subplot titles.